

Platelet GPIb is a mediator and potential interventional target for NASH and subsequent liver cancer

Malehmir, Mohsen; Pfister, Dominik; Gallage, Suchira; Szydłowska, Marta; Inverso, Donato; Kotsiliti, Elena; Leone, Valentina; Peiseler, Moritz; Surewaard, Bas G J; Rath, Dominik; Ali, Adnan; Wolf, Monika Julia; Drescher, Hannah; Healy, Marc E; Dauch, Daniel; Kroy, Daniela; Krenkel, Oliver; Kohlhepp, Marlene; Engleitner, Thomas; Olkus, Alexander

DOI:

[10.1038/s41591-019-0379-5](https://doi.org/10.1038/s41591-019-0379-5)

License:

Other (please specify with Rights Statement)

Document Version

Peer reviewed version

Citation for published version (Harvard):

Malehmir, M, Pfister, D, Gallage, S, Szydłowska, M, Inverso, D, Kotsiliti, E, Leone, V, Peiseler, M, Surewaard, BGJ, Rath, D, Ali, A, Wolf, MJ, Drescher, H, Healy, ME, Dauch, D, Kroy, D, Krenkel, O, Kohlhepp, M, Engleitner, T, Olkus, A, Sijmonsma, T, Volz, J, Deppermann, C, Stegner, D, Helbling, P, Nombela-Arrieta, C, Rafiei, A, Hinterleitner, M, Rall, M, Baku, F, Borst, O, Wilson, CL, Leslie, J, O'Connor, T, Weston, CJ, Adams, DH, Sheriff, L, Teijeiro, A, Prinz, M, Bogeska, R, Anstee, N, Bongers, MN, Notohamiprodjo, M, Geisler, T, Withers, DJ, Ware, J, Mann, DA, Augustin, HG, Vegiopoulos, A, Milsom, MD, Rose, AJ, Lalor, PF, Llovet, JM, Pinyol, R, Tacke, F, Rad, R, Matter, M, Djouder, N, Kubes, P, Knolle, PA, Unger, K, Zender, L, Nieswandt, B, Gawaz, M, Weber, A & Heikenwalder, M 2019, 'Platelet GPIb is a mediator and potential interventional target for NASH and subsequent liver cancer', *Nature Medicine*, vol. 25, no. 4, pp. 641-655. <https://doi.org/10.1038/s41591-019-0379-5>

[Link to publication on Research at Birmingham portal](#)

Publisher Rights Statement:

This document is the accepted manuscript version of a published work that appeared in final form in *Nature Medicine*. The final version of record can be found at: <https://doi.org/10.1038/s41591-019-0379-5>

This document is subject to Springer Nature re-use terms: <https://www.nature.com/authors/policies/license.html#AAMtermsV1>

General rights

Unless a licence is specified above, all rights (including copyright and moral rights) in this document are retained by the authors and/or the copyright holders. The express permission of the copyright holder must be obtained for any use of this material other than for purposes permitted by law.

- Users may freely distribute the URL that is used to identify this publication.
- Users may download and/or print one copy of the publication from the University of Birmingham research portal for the purpose of private study or non-commercial research.
- User may use extracts from the document in line with the concept of 'fair dealing' under the Copyright, Designs and Patents Act 1988 (?)
- Users may not further distribute the material nor use it for the purposes of commercial gain.

Where a licence is displayed above, please note the terms and conditions of the licence govern your use of this document.

When citing, please reference the published version.

Take down policy

While the University of Birmingham exercises care and attention in making items available there are rare occasions when an item has been uploaded in error or has been deemed to be commercially or otherwise sensitive.

If you believe that this is the case for this document, please contact UBIRA@lists.bham.ac.uk providing details and we will remove access to the work immediately and investigate.

Download date: 04. Aug. 2022

1 **Platelet GPIIb/IIIa is a mediator and potential interventional target for**
2 **NASH and subsequent liver cancer**

3 Mohsen Malehmir^{1,*}, Dominik Pfister^{2,*}, Suchira Gallage^{2,*}, Marta Szydlowska^{2,*}, Donato
4 Inverso^{3,4*}, Elena Kotsiliti^{2,5,£}, Valentina Leone^{2,6,£}, Moritz Peiseler^{7,8,£}, Bas G.J.
5 Surewaard^{8,9,10,£}, Dominik Rath¹¹, Adnan Ali², Monika Julia Wolf¹, Hannah Drescher¹², Marc
6 E. Healy¹, Daniel Dauch^{13,14}, Daniela Kroy¹², Oliver Krenkel¹², Marlene Kohlhepp¹², Thomas
7 Engleitner^{15,16,17}, Alexander Olkus^{2,18}, Tjeerd Sijmonsma², Julia Volz¹⁹, Carsten
8 Deppermann¹⁹, David Stegner¹⁹, Patrick Helbling²⁰, César Nombela-Arrieta²⁰, Anahita
9 Rafiei²⁰, Martina Hinterleitner^{13,14}, Marcel Rall¹¹, Florian Baku¹¹, Oliver Borst¹¹, Caroline L.
10 Wilson²¹, Jack Leslie²¹, Tracy O'Connor^{5,22}, Christopher J. Weston²³, David H. Adams^{23,24},
11 Lozan Sheriff²⁵, Ana Teijeiro²⁶, Marco Prinz^{27,28,29}, Ruzhica Bogeska³⁰, Natasha Anstee³⁰,
12 Malte N. Bongers³¹, Mike Notohamiprodjo³¹, Tobias Geisler³², Dominic J. Withers^{33,34}, Jerry
13 Ware³⁵, Derek A. Mann²¹, Hellmut G. Augustin^{3,4}, Alexandros Vegiopoulos³⁶, Michael D.
14 Milsom³⁰, Adam J. Rose³⁷, Patricia F. Lalor²³, Josep M. Llovet^{38,39,40}, Roser Pinyol³⁹, Frank
15 Tacke¹², Roland Rad^{15,16,17}, Matthias Matter⁴¹, Nabil Djouder²⁶, Paul Kubes^{7,8,9}, Percy A.
16 Knolle²², Kristian Unger⁶, Lars Zender^{13,14,42}, Bernhard Nieswandt¹⁹, Meinrad Gawaz¹¹, Achim
17 Weber^{1,**} and Mathias Heikenwalder^{2,5,**}

18

- 19 1. Department of Pathology and Molecular Pathology, University and University Hospital Zurich, Zurich,
20 Switzerland
- 21 2. Division of Chronic Inflammation and Cancer, German Cancer Research Center Heidelberg (DKFZ),
22 Heidelberg, Im Neuenheimer Feld 280, 69120 Heidelberg, Germany
- 23 3. Division of Vascular Oncology and Metastasis, German Cancer Research Center Heidelberg (DKFZ-
24 ZMBH Alliance), Im Neuenheimer Feld 280, 69120 Heidelberg, Germany
- 25 4. European Center of Angioscience (ECAS), Medical Faculty Mannheim, Heidelberg University,
26 Mannheim, Germany
- 27 5. Institute for Virology, Technische Universität München/Helmholtz Zentrum München, Munich, Germany
- 28 6. Research Unit of Radiation Cytogenetics, Helmholtz Zentrum München, Neuherberg Germany
- 29 7. Calvin Phoebe & Joan Snyder Institute for Chronic Diseases, Cumming School of Medicine, University of
30 Calgary, Calgary, Alberta, Canada.
- 31 8. Department of Physiology and Pharmacology Cumming School of Medicine, University of Calgary,
32 Calgary, Alberta, Canada.
- 33 9. Department of Microbiology, Immunology & Infectious Diseases, Cumming School of Medicine,
34 University of Calgary, Calgary, Alberta, Canada.
- 35 10. Department of Medical Microbiology, University Medical Center, Utrecht, the Netherlands.
- 36 11. Department of Cardiology and Circulatory Diseases, Internal Medicine Clinic III, Eberhard Karls
37 University Tübingen, Tübingen, Germany
- 38 12. Department of Medicine III, University Hospital RWTH Aachen, Aachen, Germany.
- 39 13. Department of Internal Medicine VIII, University Hospital Tübingen, 72076 Tübingen, Germany
- 40 14. Department of Physiology I, Institute of Physiology, Eberhard Karls University Tübingen, 72076
41 Tübingen, Germany
- 42 15. Center for Translational Cancer Research (TranslaTUM), Technische Universität München, 81675
43 Munich, Germany
- 44 16. Department of Medicine II, Klinikum rechts der Isar, Technische Universität München, 81675 Munich,
45 Germany.
- 46 17. German Cancer Consortium (DKTK), German Cancer Research Center (DKFZ), 69120 Heidelberg,
47 Germany
- 48 18. Medical Faculty, University of Heidelberg, Heidelberg, Germany.
- 49 19. Institute of Experimental Biomedicine, University Hospital and Rudolf Virchow Center, University of
50 Würzburg, Würzburg, Germany
- 51 20. Hematology, University Hospital and University of Zurich, Zurich, Switzerland

- 52 21. Newcastle Fibrosis Research Group, Institute of Cellular Medicine, Newcastle University, Newcastle
53 upon Tyne, Tyne and Wear NE2 4HH, UK.
- 54 22. Institute of Molecular Immunology and Experimental Oncology, Technical University of Munich,
55 Ismaningerstraße 22, 81675 Munich, Germany
- 56 23. Centre for Liver Research and National Institute for Health Research (NIHR) Birmingham Liver
57 Biomedical Research Unit, Birmingham B152TT, United Kingdom.
- 58 24. Liver Unit, University Hospitals Birmingham NHS Trust, Birmingham, UK.
- 59 25. Institute for Cardiovascular Sciences, University of Birmingham, Birmingham, United Kingdom.
- 60 26. Cancer Cell Biology Programme, Growth Factors, Nutrients and Cancer Group, Spanish National Cancer
61 Research Centre, CNIO, Madrid, Spain.
- 62 27. Institute of Neuropathology, Medical Faculty, University of Freiburg, Freiburg, Germany
- 63 28. Signalling Research Centres BIOS and CIBSS, University of Freiburg, Germany
- 64 29. Center for NeuroModulation, Faculty of Medicine, University of Freiburg, Germany
- 65 30. Division of Experimental Hematology, Deutsches Krebsforschungszentrum (DKFZ) and DKFZ-ZMBH
66 Alliance, 69120 Heidelberg, Germany; Heidelberg Institute for Stem Cell Technology and Experimental
67 Medicine (HI-STEM gGmbH), 69120 Heidelberg, Germany
- 68 31. Department of Diagnostic and Interventional Radiology, University Hospital of Tuebingen, Hoppe-Seyler-
69 Strasse 3, 72076, Tuebingen, Germany
- 70 32. Department of Cardiovascular Medicine, University Hospital, Eberhard Karls University of Tübingen,
71 Tübingen, Germany
- 72 33. Metabolic Signalling Group, MRC London Institute of Medical Sciences, Du Cane Road, London W12
73 0NN, UK
- 74 34. Institute of Clinical Sciences, Faculty of Medicine, Imperial College London, Du Cane Road, London
75 W12 0NN, UK
- 76 35. Department of Physiology and Biophysics, University of Arkansas for Medical Sciences, 4301 West
77 Markham Street, Little Rock, Arkansas 72205, USA
- 78 36. DKFZ Junior Group Metabolism and Stem Cell Plasticity, German Cancer Research Center, Heidelberg,
79 Germany
- 80 37. Nutrient Metabolism and Signalling Lab, Dept. of Biochemistry and Molecular Biology, School of
81 Biomedical Sciences, and Metabolism, Diabetes and Obesity Program, Biomedicine Discovery Institute,
82 Monash University, Clayton, 3800, Australia.
- 83 38. Mount Sinai Liver Cancer Program (Divisions of Liver Diseases, Department of Medicine, Department of
84 Pathology, Recanati Miller Transplantation Institute), Tisch Cancer Institute, Icahn School of Medicine at
85 Mount Sinai, New York, USA

86 39. Liver Cancer Translational Research Laboratory, IDIBAPS, Liver Unit, Hospital Clinic, University of
87 Barcelona, Barcelona, Catalonia, Spain; Institució Catalana de Recerca i Estudis Avançats (ICREA),
88 Barcelona, Catalonia, Spain

89 40. Institució Catalana de Recerca i Estudis Avançats (ICREA), Barcelona, Catalonia, Spain

90 41. **Institute of Pathology, University Hospital of Basel, 4003 Basel, Switzerland.**

91 42. Translational Gastrointestinal Oncology Group, German Consortium for Translational Cancer Research
92 (DKTK), German Cancer Research Center (DKFZ), Heidelberg, Germany

93

94 * share first authorship/contributed equally

95 £share second authorship/contributed equally

96 ** share last and corresponding authorship

97

98

99 **SUMMARY**

100

101 Non-alcoholic fatty liver disease ranges from steatosis to non-alcoholic
102 steatohepatitis (NASH), potentially progressing to cirrhosis and hepatocellular
103 carcinoma (HCC). Here, we show that platelet-number, platelet-activation and
104 platelet-aggregation are increased in NASH, but not in steatosis or insulin resistance.
105 Antiplatelet therapy (APT; Aspirin/Clopidogrel, Ticagrelor) but not NSAID **treatment**
106 **with Sulindac** prevented NASH and subsequent HCC development. Intravital
107 microscopy showed that liver colonization by platelets **depended** primarily on Kupffer
108 cells at early and late stages of NASH, involving hyaluronan-CD44 binding. APT
109 reduced intrahepatic platelet-accumulation and frequency of platelet-immune cell
110 interaction, thereby limiting hepatic immune-cell trafficking. Consequently,
111 intrahepatic cytokine/chemokine release, macrovesicular steatosis and liver damage
112 were attenuated. **Platelet-cargo**, platelet-adhesion and platelet-activation but not
113 platelet-aggregation **were identified** as pivotal for NASH and subsequent
114 **hepatocarcinogenesis**. In particular, platelet-derived GPIIb/IIIa **proved** critical for
115 development of NASH and subsequent HCC, independent of its reported cognate
116 ligands vWF, P-Selectin or Mac-1, offering a potential target against NASH.

117

118 INTRODUCTION

119 Non-alcoholic fatty liver disease (NAFLD) is the most common chronic liver disease
120 in high-income countries¹ and is on trajectory to become the most common indication
121 for liver transplantation in the United States^{2,3}. NAFLD ranges from simple steatosis
122 (non-alcoholic fatty liver (NAFL)) to non-alcoholic steatohepatitis (NASH), which may
123 progress to cirrhosis and ultimately hepatocellular carcinoma (HCC)^{4,5}. HCC is the
124 third most common cause of cancer-related death worldwide and is the fastest rising
125 cancer in the United States and Europe⁶⁻⁸. Major risk factors for NASH include
126 metabolic syndrome, abdominal obesity, insulin resistance, glucose intolerance or
127 type 2 diabetes mellitus and dyslipidaemia^{4,5,9,10}.

128 We previously developed a pre-clinical model of human metabolic syndrome, NASH
129 and NASH-induced HCC¹¹. In this model, intrahepatic influx of metabolically activated
130 CD8⁺ T- and NKT-cells triggers metabolic reprogramming of hepatocytes, NASH and
131 HCC development through cytokine-mediated cross-talk with hepatocytes. However,
132 the mechanisms underlying immune cell recruitment during NASH and its
133 consequences for NASH-to-HCC transition have remained unclear.

134 Platelets, produced by megakaryocytes in the bone marrow, play a fundamental role
135 in hemostasis¹², but are also crucial for pathophysiological conditions like thrombosis,
136 obesity, atherosclerosis, metastasis and stroke¹³⁻¹⁵. In addition, a growing body of
137 evidence highlights platelets as active players in liver disease and
138 inflammation^{13,16,17}. Notably, it has been reported that activated platelets contribute to
139 cytotoxic T lymphocyte (CTL)-mediated liver damage in a model of viral hepatitis^{18,19}.
140 Moreover, blocking platelet activation and aggregation by Aspirin-Clopidogrel (Asp-
141 Clo) abrogates hepatic T cell influx, subsequent liver damage and tumorigenesis
142 without affecting peripheral T cell function in viral hepatitis^{19,20}. Additionally, in a

143 recent study of NAFL (but not NASH) patients, anti-platelet therapy (APT) lowered
144 serum markers of obesity and liver damage²¹.

145 There is an unmet need for efficacious, low-risk therapies against NASH and NASH-
146 to-HCC transition. Although several drugs (e.g. decreasing blood sugar levels) are in
147 phase 2 and 3 development^{22,23}, currently no approved pharmacological therapies
148 are available **which can prevent** NASH or related pathologies. Further, the role of
149 platelets in NASH and HCC development is not well characterized. Thus, we
150 investigated whether APT and molecules involved in platelet function might **prevent**
151 NASH and NASH-induced HCC development.

152

153 RESULTS

154 Hepatic accumulation of activated platelets in NASH

155 To test whether platelets contribute to NASH development, we investigated platelet
156 number and distribution in livers of C57Bl/6 mice fed a choline-deficient, high-fat diet
157 (CD-HFD). Platelets numbers (**Fig 1a**) and aggregate size (**Fig 1b**) were significantly
158 increased compared to age-matched normal chow diet (ND)-fed controls (**Fig. 1a**),
159 **whereas platelet** counts in peripheral blood remained normal (**Supplementary Fig.**
160 **1a**). Although fibrinogen levels and prothrombin time (PT) remained unchanged,
161 activated partial thromboplastin time (aPTT) was significantly reduced
162 (**Supplementary Fig. 1a**). *Ex vivo* analyses of circulating platelets revealed no
163 significant differences in activation/aggregation responses in CD-HFD-fed compared
164 to ND-fed mice (**Supplementary Fig. 1b**). We next analyzed other dietary and
165 genetic murine NASH models (**Fig. 1c-e; Supplementary Fig. 1c,d**), including high-
166 fat, high-fructose, high-cholesterol, “Western-style” diets^{24,25} with or without trans-fat
167 (WD-HTF; WD-NTF), a “Western-style” diet with fructose (WD-FSDW)²⁶, a
168 methionine/choline-deficient diet (MCD) and an inducible knock-in mouse expressing
169 the human unconventional prefoldin RPB5 interactor (URI) in hepatocytes (hURI-
170 tetOFFhep)²⁷. All models **induced** NASH with varying degrees of NAS and fibrosis
171 (**Supplementary Fig. 1e,f**), a primary determinant of outcome in NASH^{28,29}, **and**
172 displayed a significant increase in intrahepatic platelet numbers compared to controls
173 (**Fig. 1a,c-e; Supplementary Fig. 1c,d**). Further, human NAFLD/NASH patients
174 displayed a significant increase in intrahepatic platelets in liver compared to healthy
175 controls (**Fig. 1f; Table S1**).

176 In contrast, mice fed a 45% kcal high-fat diet (HFD), displaying only steatosis, or
177 mice fed a 60% kcal HFD with low sucrose **experiencing only** simple steatosis and

178 insulin resistance³⁰, lacked **any** significant increase in intrahepatic platelet numbers,
179 **despite** increased body weight, NAS, liver damage and insulin resistance (HFD-
180 60%+LS) (**Fig. 1g,h; Supplementary Fig. 1g-i**). Intrahepatic platelet activation in
181 NASH was confirmed by electron microscopy (EM) (**Supplementary Fig. 1j**). Thus,
182 increased intrahepatic platelet number, platelet aggregation and platelet activation
183 **were specific to NASH**.

184 **Asp-Clo** treatment is an **APT** currently used in several diseases (e.g. to prevent
185 coronary stent thrombosis)³¹. We first addressed whether **CD-HFD-fed** mice would
186 respond to APT. Compared to untreated **CD-HFD-fed** mice, Asp-Clo-treated mice
187 displayed significantly lower intrahepatic platelet numbers (**Supplementary Fig. 1k-**
188 **m**), **as well as reduced platelet aggregation and activation** (**Supplementary Fig. 1n**).

189 To investigate the effects of APT on human NAFLD, we **performed a pilot case-study**
190 (German Clinical Trials Register (DRKS) 587/2016BO2) with **patients at risk for**
191 **NAFLD** (BMI>30 and/or diabetes mellitus type II) undergoing a heart catheter
192 procedure. Depending on the outcome of the catheter procedure, one of three
193 outcomes was carried out: **(1)** Patients received dual antiplatelet therapy (DAPT) for
194 at least 6 months if a coronary stent was implanted. **(2)** ASA monotherapy was given
195 for at least 6 months if coronary artery disease (CAD) was present but stent
196 implantation was not indicated. **(3)** No anti-aggregation therapy was given if coronary
197 artery disease was absent. None of the patients included received long-term
198 treatment with ASA or P2Y12 before study inclusion (**Supplementary Fig. 1o; Table**
199 **S2**). **In this pilot case-study of 24 individual patients/observations**, platelet function
200 analyses revealed that patients generally responded well to APT (**Supplementary**
201 **Fig. 1p**), although serum total cholesterol, LDL- and HDL- cholesterol levels
202 remained unchanged (**Supplementary Fig. 1p,q**). For control, we investigated
203 patients without APT (**Table S2**). NAFLD patients underwent liver MRI, liver

204 ultrasound and serum analysis at study inclusion and after 6 months of follow-up.
205 APT-treated NAFLD patients showed significantly reduced liver volume and liver fat
206 mass (**Supplementary Fig. 1r-t**). Patients who received a new therapy with ASA or
207 DAPT were diagnosed with CAD. The standard treatment in patients with CAD
208 includes statins. Hence, patients who received a new anti-aggregation therapy were
209 usually treated with a new statin treatment if statins were not already administered on
210 a regular basis and if contra-indications were absent. Thus, statins might present a
211 significant confounder in the actual pilot case-study, which we tried to address by
212 performing a linear regression analysis. Since the study collective was small, we
213 included age, gender, anti-aggregation and new statin treatment into the regression
214 analysis. For the course of liver fat, we found the strongest associations for anti-
215 aggregation ($b=-0.334$, 95% CI $-4.719-1.197$, $p=0.226$), whereas initiation of a new
216 statin treatment showed weaker associations ($b=-0.095$, 95% CI $-3.551-2.526$,
217 $p=0.726$). For the course of liver volume, we found associations for anti-aggregation
218 ($b=-0,454$, 95% CI $-0.170-0.006$, $p=0.066$) stronger compared to initiation of a new
219 statin treatment ($b=0.047$, 95% CI $-0.084-0.101$, $p=0.847$). This indicated that effects
220 of anti-aggregation were stronger than statin administration. Notably, $n=4$ patients
221 showed significant reductions in liver fat content and/or liver volume without new
222 statin therapy. However, there was a trend towards effect of anti-aggregation without
223 being statistically significant. Higher BMI did not significantly affect liver fat or liver
224 volume.

225

226 **Asp-Clo treatment attenuates NASH and NASH-associated conditions**

227 We next investigated whether Asp-Clo (adjusted to the body weight) affects NASH or
228 HCC development in mice receiving ND, CD-HFD or CD-HFD with Asp-Clo for 12

229 months. Weight gain over time was significantly higher in CD-HFD and CD-HFD/Asp-
230 Clo-fed mice compared to ND-fed controls (**Fig. 2a**). Similar to body weight,
231 epididymal fat (eWAT) weight was not different to CD-HFD in CD-HFD/Asp-Clo-fed
232 mice (**Supplementary Fig. 2a**). Low platelet numbers were found in eWAT and
233 remained unaltered (**Supplementary Fig. 2b,c**). CD3⁺ T-cell infiltration was
234 significantly reduced by Asp-Clo (**Supplementary Fig. 2c**). RNAseq analysis of
235 eWAT from ND- and CD-HFD-fed mice revealed a different gene expression pattern
236 resulting in the spatial separation in the PCA plot. Analysis of the most differentially
237 expressed genes between diets showed upregulation of pathways involved in
238 immune signaling, cell-cell interactions and extracellular matrix regulation in eWAT
239 from CD-HFD-fed mice. In contrast, eWAT of CD-HFD fed-mice showed a significant
240 downregulation in pathways involved in metabolism and antioxidant response
241 (**Supplementary Fig. 2d**). ALT, AST, liver/body weight ratio, platelet numbers and
242 aggregation state were significantly lower in livers of mice fed CD-HFD/Asp-Clo for 6
243 and 12 months (**Fig. 2b; Supplementary Fig. 1k-n; Supplementary Fig. 2e,f**). Asp-
244 Clo significantly improved glucose tolerance (**Fig. 2c**), reduced liver triglycerides
245 (**Fig. 2d**), and attenuated serum total cholesterol, LDL- and HDL- cholesterol levels
246 (**Fig. 2e; Supplementary Fig. 2g,h**). Several genes involved in fatty acid β -oxidation,
247 lipolysis and cholesterol metabolism are dysregulated during NASH development¹¹.
248 Asp-Clo treatment prevented downregulation of genes from all three groups (**Fig. 2f**).
249 CD-HFD/Asp-Clo-fed mice lacked statistically significant changes in oxygen
250 consumption, respiratory exchange ratio (RER), physical activity or in food and water
251 intake compared to CD-HFD-fed mice (**Fig. 2g,h; Supplementary Fig. 2i**). These
252 data were corroborated in WD-HTF fed mice (**Supplementary Fig 2. j,k**).

253 To analyze platelet activation, P-selectin, a marker of α -granule release, and integrin
254 α IIb β 3 activation were analyzed by flow cytometry. In Asp-Clo-treated CD-HFD mice,

255 circulating platelets showed markedly reduced integrin $\alpha\text{IIb}\beta\text{3}$ activation and P-
256 selectin exposure compared with ND and CD-HFD platelets in response to all tested
257 agonists (**Supplementary Fig. 2l**), suggesting that Asp-Clo treatment effectively
258 reduced platelet activation. Levels of major platelet surface glycoproteins were
259 unchanged (**Supplementary Fig. 2m**).

260 MRI-analysis revealed subcutaneous/abdominal fat accumulation in CD-HFD and
261 CD-HFD/Asp-Clo treated mice, but not in ND-fed controls (**Fig. 2i**). However, liver
262 steatosis was ameliorated or even prevented by Asp-Clo treatment in CD-HFD mice
263 (**Fig. 2i**). In contrast, untreated CD-HFD-fed mice displayed histopathological
264 features of NASH, including liver fat deposition (Sudan red⁺ areas), fibrosis, damaged
265 hepatocytes and lobular inflammation including satellitosis (**Fig. 2j, 2k,**
266 **Supplementary Fig. 2n,o**). We concluded that Asp-Clo treatment effectively
267 prevented NASH development.

268 **Asp-Clo treatment abrogates intrahepatic immune-cell infiltration and inhibits** 269 **NASH-induced HCC**

270 In addition to hepatic infiltration of CD3⁺CD8⁺ T cells, CD11b⁺ MHCII⁺ myeloid cells
271 and Ly-6G⁺ granulocytes are increased in CD-HFD-fed mice, similar to human NASH
272 patients¹¹. Immune cell infiltration was reduced in 6-month and 12-month CD-
273 HFD/Asp-Clo-treated mice (**Fig. 3a**). Flow cytometry demonstrated strong reduction
274 in total number, effector differentiation (CD8⁺CD62L⁻CD44⁺CD69⁺) and proportion of
275 CD4⁺/CD8⁺ and NKT-cells (**Fig. 3b,c**). B-cells remained unchanged in 6 months ND,
276 CD-HFD or CD-HFD/Asp-Clo fed mice (**Supplementary Fig. 3a,b**).

277 Analyses of several **potentially carcinogenic** inflammatory signaling pathways
278 activated under CD-HFD were dampened by Asp-Clo (**Fig. 3d** and **Supplementary**

279 **Fig. 3c**). Asp-Clo significantly reduced CD11b⁺F4/80^{hi} Kupffer cells (KCs) in WD-HTF
280 livers (**Supplementary Fig. 3d-k**). An unbiased t-distributed stochastic neighbor
281 embedding (t-SNE)-based clustering approach identified 9 myeloid sub-clusters
282 (**Supplementary Fig. 3h,i** and **Table S3**). Asp-Clo significantly reduced the
283 abundance of cluster 6, characterized by a high expression of CD11b, F4/80 and
284 Gr1, closely resembling CD11b⁺F4/80⁺ monocyte-derived macrophages (MoMFs).
285 Further, a multiplex gene expression analysis for FACS-isolated Ly6C⁺ MoMFs,
286 LY6C⁻ MoMFs and KCs was performed. Principal component analysis of 561 genes
287 revealed similar Ly6C⁺ MoMFs and Ly6C⁻ MoMFs in NASH-diet-fed mice with and
288 without Asp/Clo treatment. However, KCs from WD-HTF/Asp-Clo livers clustered
289 more closely to ND KCs than WD-HTF (**Supplementary Fig. 3h-k**). This indicates
290 that Asp-Clo influences the KC compartment. Taken together, these data indicate
291 that Asp-Clo treatment attenuated KC activation, alongside reduced inflammatory
292 myeloid cell infiltration in the injured liver. Altogether, Asp-Clo prevented NASH,
293 reduced intrahepatic immune cell influx and dampened pathways potentially
294 supporting hepatocarcinogenesis³².

295 Next, we studied the effects of Asp-Clo treatment on CD-HFD-induced HCC¹¹. 13 out
296 of 51 CD-HFD livers (~25%) displayed macroscopically visible tumors by 12 months
297 (**Fig. 3e-g**). In contrast, CD-HFD/Asp-Clo-treated mice lacked macro- and
298 microscopically visible liver tumors (**Fig. 3e-g; Supplementary Fig. 3l**). CD-HFD-fed
299 mice treated with a lower dose of Asp-Clo (according to the initial body weight and
300 not further adjusted to diet/age-related weight gain) developed significantly fewer
301 HCC (3/52) compared to untreated CD-HFD-fed mice (13/51) (**Supplementary Fig.**
302 **3m**). Therefore, the dose of Asp-Clo continuously adjusted to the body weight is
303 critical to fully prevent HCC.

304

305 **Asp/Clo dampens hepatic cytokine expression, platelet-liver endothelium and**
306 **platelet-immune cell interaction**

307 Gene expression and signaling pathway analyses of ND, CD-HFD and WD-HTF
308 livers revealed a significant induction in gene expression profiles involved in platelet
309 activation, aggregation and degranulation (**Extended Data-Fig. 1a-i**). Moreover,
310 NASH-related enrichment of genes was associated with expression of TNF-
311 superfamily members, cytokine/chemokine production and chemotaxis^{11,27}
312 (**Extended Data-Fig. 1a-i**). Asp-Clo treatment significantly attenuated the latter,
313 some of which are also released from activated platelets (e.g. CCL5, TGF β)
314 (**Extended Data-Fig. 1j**)³³.

315 Coupling high-resolution confocal microscopy and 3D-reconstruction of liver
316 sinusoids enabled visualization and quantification of platelet interactions with the liver
317 endothelium and immune cells. Asp-Clo reduced NASH-related increased interaction
318 of platelets with the liver endothelium, T-cells and innate immune cells (**Extended**
319 **Data-Fig. 1k-q**).

320 To exclude COX2-dependent effects of Asp-Clo, we used another NSAID/COX1/2
321 inhibitor, Sulindac. CD-HFD/Sulindac-treated mice exhibit obesity, no significant
322 changes in liver/body weight ratio, hepatic triglycerides, glucose tolerance, no
323 significant alteration in gene expression involved in metabolism, severe steatosis and
324 increased liver damage comparable to CD-HFD treated mice (**Extended Data-Fig.**
325 **2a-f**). Thus, Asp/Clo-mediated effects on NASH are COX-independent.

326 To corroborate our results with another platelet inhibitor, CD-HFD-fed mice were
327 treated with Ticagrelor (CD-HFD/Ticagrelor), an FDA-approved direct and reversible

328 antagonist of the platelet P2Y₁₂ receptor³⁴ for coronary artery disease used in the
329 clinic (e.g. with ASA after coronary stent implantation in patients presenting with an
330 acute coronary syndrome without increased bleeding risk)³⁵. Intrahepatic platelet
331 number, platelet/liver endothelium coverage, platelet aggregation, liver damage, liver
332 triglycerides and serum cholesterol levels were significantly reduced in Ticagrelor-
333 treated mice, **whereas VLDL secretion was not affected (Extended Data-Fig. 3a-h).**
334 **Expression of genes involved in cholesterol metabolism, 'de novo' lipogenesis and**
335 **lipid storage was unchanged by the treatment, while downregulation** of several
336 genes involved in fatty acid oxidation and lipolysis that occurs during CD-HFD
337 **(Extended Data-Fig. 3i,j)** as well as histopathological features of NASH were
338 prevented by Ticagrelor **(Extended Data-Fig. 3k-m)**. Total numbers, activation and
339 proportion of CD4⁺/CD8⁺, CD8⁺CD62L⁻CD44⁺CD69⁺ and CD3⁺NK1.1⁺ cells were also
340 reduced **(Extended Data-Fig. 3n,o)**. In contrast to liver tissues, increased
341 expression of genes involved in inflammation and fibrosis was found in eWAT from
342 CD-HFD or WD-HTF mice receiving Asp-Clop or Ticagrelor **(Extended Data-Fig.**
343 **3p)**. **This indicate that APT is beneficial specifically to the liver, affecting not only**
344 **intrahepatic platelets and immune-cell infiltration, but also improving hepatic steatosis**
345 **by maintaining normal expression of genes involved in lipid catabolism.**

346

347 We next investigated whether Ticagrelor would affect NASH-HCC transition.
348 **Compared** to untreated CD-HFD mice, Ticagrelor treatment significantly reduced
349 HCC development. One **tumor** was detected in 29 livers of CD-HFD/Ticagrelor-
350 treated mice **(Extended Data-Fig. 3q)**. The therapeutic potential of Ticagrelor was
351 tested in CD-HFD mice with fully established NASH (4 months CD-HFD), followed by
352 8-weeks of Ticagrelor treatment with CD-HFD. Intrahepatic platelet numbers, NAS,
353 liver damage were reduced, and no difference in glucose tolerance was found

354 (**Extended Data-Fig. 3r,s**), or effect on the blood immune cells populations was
355 observed (**Extended Data-Fig. 3t**). Similar results were obtained with therapeutic
356 Ticagrelor treatment in the context of a WD-HTF including of fibrosis; no difference in
357 whole body metabolism was found upon Ticagrelor treatment in CD-HFD or WD-HTF
358 (**Extended Data-Fig. 3u-x**).

359

360 **Early platelet recruitment in fatty liver correlates with liver damage, hepatocyte** 361 **swelling and reduced sinusoidal diameter**

362 To understand the dynamics of intrahepatic platelet recruitment/attachment during
363 the initial events of NAFL **preceding** NASH, we performed intravital microscopy in
364 CD-HFD or WD-HTF-fed mice over 4, 5, 6 and 8 weeks post-diet induction (pdi) (**Fig.**
365 **4a; Supplementary Fig. 4a-c**). Platelets were the first non-resident cell type to
366 populate the liver at ≤ 4 weeks pdi in both CD-HFD and WD-HTF (**Fig. 4a-d;**
367 **Supplementary Fig. 4a-c**). Platelets progressively aggregated and increased in
368 number in liver sinusoids over 8 weeks in the absence of significantly elevated CD3⁺
369 T-cells or Ly6G⁺ granulocytes (**Fig. 4a-d; Supplementary Fig. 4a-c**). Even at this
370 early stage, mild steatosis, reduced sinusoidal diameter and hepatocyte swelling
371 were observed (**Fig. 4e,f; Supplementary Fig. 4e**). NAS, liver triglycerides were
372 increased in CD-HFD and WD-HTF (**Fig. 4g,h; Supplemental Fig. 4d-f**). Platelets
373 interacted primarily with Kupffer cells, as determined by 3D high-resolution
374 reconstruction (**Fig. 4i**). Although intrahepatic granulocyte numbers remained
375 unaltered in the first 8 weeks pdi, granulocytes might still support intrahepatic platelet
376 recruitment and NAFL/NASH induction. Administration of anti-Ly6G antibodies via
377 **osmotic** pumps for 8 weeks to CD-HFD-fed mice did not reduce intrahepatic platelet
378 numbers but successfully reduced granulocytes. Experiments revealed no significant

379 role of granulocytes in the early development of NAFL and borderline NASH
380 (**Supplementary Figure 4g-k**).

381 We next screened for possible adhesion molecules/danger markers responsible for
382 early platelet attachment/recruitment. We found progressive induction of the
383 extracellular matrix component hyaluronan (HA) **co-localizing with** hepatocytes,
384 Kupffer cells and, to lesser degree, on LSECs (**Fig. 4j**).

385

386 **Kupffer cell-dependent platelet recruitment involving hyaluronan-CD44 binding**
387 **supports early and advanced stages of NAFL including NASH**

388 To investigate the functional role of Kupffer cells and molecules involved in platelet-
389 LSEC/immune-cell interaction (e.g. hyaluronan, CD44) in borderline NASH, CD-HFD
390 or WD-HTF-fed mice were treated with clodronate liposomes (CLL), control
391 liposomes (CL), hyaluronidase (HYAL), HYAL/CLL (double treatment), CD44-
392 binding/HA-blocking AB (clone KM81) or CD44-binding/HA-non-blocking AB (clone
393 IM7), for control (**Fig. 5a, Supplementary Fig. 5a,b**). CLL and CLL/HYAL, but not CL
394 treatment reduced Kupffer cell numbers in CD-HFD- and WD-HTF-fed mice (**Fig. 5b,**
395 **Supplementary Fig. 5c,d**). CLL and HYAL reduced NAS significantly in CD-HFD
396 and WD-HTF-fed mice (**Fig. 5b, Supplementary Fig. 5d**). CLL and HYAL treatments
397 significantly reduced intrahepatic platelets (**Fig. 5c**), a significant reduction in liver
398 damage was found following HYAL but not CLL (**Fig. 5d**). Combined treatment with
399 both CLL/HYAL did not result in further decrease of platelet numbers
400 (**Supplementary Fig. 5f**). Similar data (platelet reduction, NAS reduction) with CLL
401 treatment were obtained using WD-HTF mice, although ALT levels remained
402 elevated (**Supplementary Fig. 5d,e**). In addition, treatment with a CD44-binding/HA-

403 blocking, but not with a CD44-binding/HA non-blocking antibody led to a reduction in
404 NAS and liver damage (**Fig. 5e-g**).

405 Notably, significantly reduced NAS, platelet accumulation, triglycerides, and liver
406 damage by CLL-treatment in mice fed CD-HFD for 6 months demonstrate **a potential**
407 therapeutic **effect of** CLL even in a short treatment scheme (**Fig. 5 h,i;**
408 **Supplementary Fig. 5h,i**). These data **imply** that Kupffer cells, hyaluronan and
409 CD44 are important players in the early and advanced stages of NAFL, including
410 NASH.

411 **Platelet cargo is indispensable for NASH development**

412 Platelets release bioactive factors from intracellular granules in response to cellular
413 activation. During thrombo-inflammatory reactions, the mostly proteinous
414 components of α -granules are essential for immune cell recruitment and tissue
415 damage³⁶. *Nbeal2* knockout mice (*Nbeal2*^{-/-}), which lack α -granules in platelets and
416 are thus protected from thrombosis and thrombo-inflammatory tissue damage³⁷⁻³⁹
417 were on CD-HFD for 6 months. CD-HFD-fed *Nbeal2*^{-/-} displayed no significant
418 difference in intrahepatic platelet number or aggregation and gained weight similarly
419 to CD-HFD-fed controls (**Fig. 5j; Supplementary Fig. 5j**). Still, significantly lower
420 serum ALT and AST levels were found in CD-HFD-fed *Nbeal2*^{-/-} mice compared to
421 CD-HFD-fed mice (**Fig. 5k**). This was paralleled by a significant decrease in liver
422 triglycerides, lower serum cholesterol (**Fig. 5l,m**), and improved glucose tolerance in
423 CD-HFD-fed *Nbeal2*^{-/-} mice (**Supplementary Fig. 5k**). Deregulation of lipid
424 metabolism genes found in CD-HFD livers was partially prevented in CD-
425 HFD/*Nbeal2*^{-/-} (**Supplementary Fig. 5l**). CD-HFD *Nbeal2*^{-/-} livers lacked steatosis,
426 NASH, **and displayed a** reduced NAS (**Fig. 5n; Supplementary Fig. 5m**).
427 Suppression of NASH in *Nbeal2*^{-/-} mice on CD-HFD was corroborated by significant

428 diminution of lipid content (**Fig. 5o**). In line, decreased T-cell infiltration, neutrophil
429 accumulation and macrophage activation were found in *Nbeal2^{-/-}* mice on CD-HFD
430 (**Supplementary Fig. 5n**). Together, these results indicated that platelet α -granule
431 components contribute to NASH.

432 CD-HFD-induced NASH could not be rescued in mice lacking the GPIIb subunit of
433 the platelet fibrinogen receptor GPIIb/IIIa (integrin $\alpha 2\beta 3$; *Itga2b^{-/-}* mice) which harbors
434 activatable platelets unable to aggregate (**Extended Data-Fig. 4**). This is in
435 agreement with a recent study indicating that deletion of the platelet integrin $\alpha 2\beta 3$
436 binding motif of fibrinogen did not alter NASH⁴⁰.

437 Moreover, mice lacking the activating platelet collagen receptor glycoprotein VI
438 (GPVI; *Gp6^{-/-}*)⁴¹, the platelet-derived C-type lectin-like receptor 2 (*Clec-2^{-/-}*) or the
439 hematopoietic-specific podoplanin (*Pdpr^{-/-}*) all developed NASH and NASH-
440 associated conditions upon CD-HFD feeding (**Extended Data-Fig. 5-6**).

441 Mucosal vascular addressin cell adhesion molecule 1 (MAdCAM-1) was recently
442 discovered as an important player in NASH⁴². Animals with genetic inactivation of
443 MAdCAM-1 presented lower NAS and less liver damage after 6-month of WD-HTF⁴².
444 We analyzed livers of WD-HTF-fed mice lacking MAdCAM-1 (*MAdCAM-1^{-/-}*), L-
445 selectin (*L-sel^{-/-}*), integrin beta7 (*$\beta 7^{-/-}$*) and both L-selectin and integrin beta7 (*L-
446 sel/ $\beta 7^{-/-}$*). *MAdCAM-1^{-/-}* mice displayed significantly reduced intrahepatic platelet
447 numbers correlating with a partial protection from NASH (**Extended Data-Fig. 7a,b**).
448 In contrast, **deletion** of MAdCAM-1 ligands integrin beta7, L-selectin and L-
449 selectin/integrin beta7 did not affect intrahepatic platelet numbers or platelet
450 aggregation and did not or only partially prevent NASH (**Extended Data-Fig. 7a-b**).

451

452 **Platelet GPIb α and α -granules are required to induce NASH**

453 Our data demonstrate that intrahepatic interaction of platelets with Kupffer cells,
454 involving hyaluronan/CD44 binding and platelet cargo-function, but not platelet
455 aggregation contribute to NASH. Platelet-derived GPIb α has been **implicated in**
456 platelet attachment and activation⁴³

457 We thus hypothesized that GPIb α might mediate **early** platelet-trafficking/activation in
458 NASH livers⁴³. We first analyzed the interaction of GPIb α with parenchymal and non-
459 parenchymal liver cells (LSECs; Kupffer cells etc.) in NASH. 3D reconstruction
460 revealed **that the** most abundant interactions **of** GPIb α ⁺ platelets **were with** Kupffer
461 cells **and** less so with LSECs in mouse and human NASH samples (**Fig. 6a,b;**
462 **Supplementary Fig. 6a**).

463 Thus, we blocked the major ligand binding domain of GPIb α in 6-months CD-HFD-
464 fed mice **therapeutically** using Fab fragments of the anti-GPIb α antibody, pop/B⁴⁴ for
465 5 weeks. Notably, this short **therapeutic** treatment significantly reduced intrahepatic
466 platelet accumulation in the presence of CD-HFD (**Fig. 6c,d**). Consequently,
467 steatosis, NAS, liver damage, liver triglycerides and intrahepatic immune-cell
468 infiltration were reduced; fibrosis was dampened (**Fig. 6c-h; Supplementary Fig. 6b-**
469 **d**). In addition, anti-GPIb α antibody treatment reduced intrahepatic protein
470 expression of several pro-inflammatory and homeostatic cytokines/chemokines,
471 including CCL5, CCL6, ICAM-1, P-selectin and CD40, linking intrahepatic platelet
472 activation and Nbeal2-dependent cargo release with mediators of inflammation
473 (**Supplementary Fig. 6e**).

474 We next tested whether therapeutic anti-GPIb α antibody treatment would prevent
475 fatty liver to NASH transition in early disease progression (e.g. after 6 week CD-HFD;

476 see also Figure 4). However, these treatments did not ameliorate NAFL/ borderline
477 NASH - most likely due to lack or low expression of yet unidentified GPIb α ligands at
478 early disease stages (**Supplementary Fig. 6f,g**). These data highlight distinct
479 mechanisms of platelet recruitment in early versus established NAFL/borderline
480 NASH – still involving Kupffer cells at both disease stages.

481 To corroborate the above data in a genetic model, we fed transgenic mice expressing
482 an IL-4 α /GPIb α fusion-protein in a *GPIb α ^{-/-}* background⁴⁵ in which the ligand-binding
483 ectodomain of GPIb α is replaced by the α -subunit of the human IL-4 receptor
484 (*hIL4 α /GPIb α -Tg*)⁴⁵ with a CD-HFD for 6 months. Remarkably, platelet aggregate
485 size, platelet area and platelet-liver endothelium coverage were significantly lower in
486 CDHFD-fed *hIL4 α /GPIb α -Tg* mice compared to CD-HFD-fed C57Bl/6 controls
487 (**Supplementary Fig. 6h-j**). Both *hIL4 α /GPIb α -Tg* and C57Bl/6 mice gained weight
488 similarly when fed CD-HFD (**Supplementary Fig. 6k**). Serum cholesterol, liver
489 triglycerides, serum ALT and AST levels were significantly lower in CD-
490 HFD/*hIL4 α /GPIb α -Tg* mice (**Fig. 6i,j; Supplementary Fig. 6l**), accompanied by less
491 LDL- and HDL-cholesterol (**Supplementary Fig. 6l**). Similarly, dysregulated mRNA
492 expression of lipid metabolism-related genes in CD-HFD-fed C57Bl/6 livers was
493 prevented in CD-HFD/*hIL4 α /GPIb α -Tg* livers (**Supplementary Fig. 6m**). We also
494 observed strong and significant reductions in intrahepatic CD8⁺ T- and NKT-cells by
495 flow cytometry analysis (**Fig. 6k**). In line, CD3⁺ and reduced macrophage -
496 influx/activation were observed by immunohistochemistry (**Supplementary Fig. 6n-**
497 **o**). CD-HFD/*hIL4 α /GPIb α -Tg* mice showed lower intrahepatic protein expression of
498 several pro-inflammatory and homeostatic cytokines/chemokines, including CCL5,
499 CD40 and TNFRSF11B (**Supplementary Fig. 6p**), mechanistically linking platelet
500 attachment/activation, cytokine/chemokine expression to efficient intrahepatic

501 immune-cell attraction. CD-HFD/hIL4 α /GPIb α -Tg mice lacked histological features of
502 NASH, paralleled by a reduction in lipid accumulation and absence of macro-
503 vesicular steatosis analyzed by H/E and Sudan red staining (**Fig. 6l-o**).

504 Notably, mice lacking the major platelet adhesion receptors P-selectin (*Selp*^{-/-})⁴⁶, von-
505 Willebrand-factor (*vWF*^{-/-})⁴⁷ or Mac-1 (*Mac1*^{-/-})⁴⁸, the **known** ligands of GPIb α ,
506 displayed full-blown NASH after six months of CD-HFD (**Extended Data-Fig. 8-10**).

507 Finally, we investigated whether hIL4 α /GPIb α -Tg mice would develop HCC upon
508 long-term CD-HFD. Of note, *hIL4 α /GPIb α -Tg* mice receiving CD-HFD for 12 months
509 displayed significantly lower fibrosis, serum ALT levels, and lacked any macro- or
510 microscopical evidence of HCC (**Fig. 6p-u**).

511

512 **DISCUSSION**

513 It is becoming increasingly clear that beyond their central role in hemostasis and
514 wound repair after vascular injury⁴⁹, platelets are key players in multiple
515 pathophysiological conditions^{16-18,20}, including cytotoxic T lymphocyte (CTL)-
516 mediated liver damage and associated pathologies¹⁸. Here, we identified Kupffer
517 cells as key players in intrahepatic platelet recruitment in early and advanced stages
518 of NAFL/borderline NASH and NASH. In early NAFL/borderline NASH, hyaluronan
519 and CD44 binding are also involved. In late NASH, GPIIb α expressed by platelets
520 appeared to be primarily involved in the interaction of platelets with Kupffer cells and
521 in the maintenance of NASH. Thus, Kupffer cells play distinct roles in intrahepatic
522 platelet recruitment at different NAFLD stages.

523 We found no evidence for a role of platelet-derived GPIIb/IIIa (*Itga2b*^{-/-} mice) in
524 NASH, suggesting platelet activation and adhesion are important, whereas platelet
525 aggregation is dispensable.

526 What is the function of platelets recruited to the liver? Our results indicate a major
527 contribution of the platelet-cargo function (α -granule components) in NASH
528 progression, exemplified by the marked protection of *Nbeal2*^{-/-} mice. The exact nature
529 of platelet-derived α -granule constituents is currently unclear. However, several
530 chemokines/cytokines were reduced upon therapeutic anti-GPIIb α antibody treatment
531 in the liver. This suggests that the number and activation state of intrahepatic
532 platelets directly or indirectly correlates with an increase in immune-cell attracting
533 chemokines/cytokines.

534 The key role of GPIIb α in NASH identified in this study parallels a similarly vital
535 function of this receptor in the development of experimental autoimmune
536 encephalomyelitis (EAE), where it orchestrates the recruitment of leukocytes to the

537 inflamed CNS⁵⁰. Our results, similar to the EAE study, argue against a key role of the
538 three known cognate interaction partners of GPIb α : P-selectin, vWF and Mac-1
539 ^{48,51,52} and point to a GPIb α -activation-dependent pro-inflammatory function of α -
540 granules in intrahepatic immune-cell attraction.

541 **Selectins have also** been shown to be dispensable for leukocyte recruitment **in**
542 inflamed liver microvasculature⁵³. Other interaction partners might be involved (e.g.
543 coagulation factors XI, XII). It is also conceivable that GPIb α exerts its function in
544 disease development independent **of an ectopic ligand**⁵⁴. Moreover, due to the
545 complex pathogenesis underlying NASH, it is plausible that GPIb α is not the only
546 molecule involved. **Mice** lacking MAdCAM-1 (*MAdCAM-1*^{-/-}) **also** showed significantly
547 reduced intrahepatic platelet infiltration, but the exact mechanisms by which this
548 **occurs is unknown**.

549 **Cholesterol also** plays a pivotal role during NASH pathogenesis by inducing hepatic
550 lipotoxicity⁵⁵. Notably, different Western diets (e.g., HTF/NTF) with high cholesterol
551 recapitulated platelet-dependent phenotypes (increased intrahepatic platelets and
552 responsiveness to therapeutic APT) described in the CD-HFD; however, with a more
553 pronounced NASH phenotype **with** higher NAS and fibrosis.

554 **Of note**, platelets and platelet-derived GPIb α are potential therapeutic targets of
555 NASH and subsequent HCC development. **Although GPIb α -antibody treatment**
556 **induces prolonged bleeding-time, it does not induce spontaneous bleeding**⁴⁴, **as only**
557 **one GPIb α epitope is blocked, leaving receptor function largely intact. Thus, GPIb α**
558 **antibody is a potentially safe new treatment modality against a metabolic disease of**
559 **major public health burden**^{4,9}. So far, there is no drug treatment available specifically
560 targeting NASH. The use of pioglitazone (most promising drug so far/off-label outside
561 T2DM because of side-effects) or vitamin E (better safety/tolerability in the short-

562 term) or combination thereof could be used for NASH treatment^{4,56}. Other agents
563 such as obeticholic acid have also improved histological features of NASH, although
564 data with respect to their long-term benefits are still being awaited⁵⁷. Combined
565 therapies for NASH treatment are currently being pursued, as only a subset of
566 patients responds well to monotherapies⁵. This might be overcome by stratifying
567 more responsive patients to a given monotherapy or by utilizing multi-target drugs. A
568 viable approach might be a metabolic target in combination with an anti-inflammatory
569 or anti-fibrotic drug, such as APT and statins, as described in our pilot case-study.
570 Nevertheless, given that APT or anti-GPIIb/IIIa treatment attenuated metabolic
571 dysfunction, inflammation and fibrosis, these constitute potential monotherapies
572 against NASH. Although a risk for bleeding cannot be excluded for both, which
573 warrants careful monitoring, a single substance therapy is expected to harbor a lower
574 risk of side effects compared to combined therapies.

575 Given that only a proportion of patients with NAFLD progress to NASH and HCC, the
576 question remains at which stage of NAFLD such treatments should be initiated.
577 Future studies are needed not only to identify novel druggable targets for
578 NASH/HCC, but also to identify non-invasive biomarkers for detection of early
579 NAFLD and NASH, when it is still amenable to therapeutic intervention. In line, it was
580 recently demonstrated that higher serum ALT correlated with HCC development not
581 only in a mouse model of chronic liver cell damage, but also in patients with chronic
582 liver disease of diverse etiology including NASH^{11,58}.

583 Prophylactic APT, commonly used for acute and long-term treatment of coronary
584 artery disease⁵⁹, and Ticagrelor attenuate NASH and NASH-induced HCC¹⁶. In
585 contrast, Sulindac did not prevent NASH in mice. Thus, rather than NSAIDs in

586 general, therapies that specifically block intrahepatic platelet accumulation/platelet
587 function seem to be required to prevent NASH and NASH-associated conditions.

588 For NASH, we also **observed** a therapeutic effect of APT **in preventing** NASH-
589 triggered HCC (although potential therapeutic effects of APT in the context of pre-
590 existing HCC was not tested)⁶⁰. Similarly, we have observed a therapeutic anti-NASH
591 effect of anti-GPIIb α antibody treatment. Remarkably, in both cases therapeutic
592 treatment partially dampened fibrosis.

593 Furthermore, in a small prospective human cohort study, APT reduced liver volume
594 and liver fat accumulation in NAFLD patients, supporting the results of our murine *in*
595 *vivo* experiments. The results of **this pilot case-study, being a starting point for further**
596 **studies have to be taken with caution as it is currently underpowered. Although a**
597 **multivariate analysis on a small patient cohort inherently warrants careful**
598 **interpretation, our data have shown that effects of anti-aggregation were stronger**
599 **than those of statin administration.**

600 In our study, NASH **prevention** (e.g. by two distinct APTs: Ticagrelor and Asp/Clo; in
601 hIL4 α /GP1b α -Tg mice) ultimately suppressed subsequent HCC formation, mostly
602 because the pro-carcinogenic NASH-related environment (e.g. intrahepatic
603 inflammation, signaling, hepatocyte damage) was lacking. Moreover, treatment with
604 anti-GPIIb α antibody or depletion of Kupffer cells **abrogated** NASH **therapeutically**.
605 These approaches might have an important impact for chemo-preventive strategies,
606 **which still are lacking against NASH**. Thus, our findings provide a rationale for APT,
607 P2Y12 antagonists or reagents directly blocking platelet-derived GPIIb α or related
608 pathways as possible therapeutic approaches for NASH patients not only to
609 prevent/revert NASH but also to **prevent** NASH to HCC transition.

610

611 **References**

- 612 1. Fleet, S.E., Lefkowitz, J.H. & Lavine, J.E. Current Concepts in Pediatric Nonalcoholic Fatty
613 Liver Disease. *Gastroenterol Clin North Am* **46**, 217-231 (2017).
- 614 2. European Association for the Study of the, L., European Association for the Study of, D. &
615 European Association for the Study of, O. EASL-EASD-EASO Clinical Practice Guidelines for
616 the management of non-alcoholic fatty liver disease. *J Hepatol* **64**, 1388-1402 (2016).
- 617 3. Younossi, Z., *et al.* Global Perspectives on Non-alcoholic Fatty Liver Disease and Non-
618 alcoholic Steatohepatitis. *Hepatology* (2018).
- 619 4. Brunt, E.M., *et al.* Nonalcoholic fatty liver disease. *Nat Rev Dis Primers* **1**, 15080 (2015).
- 620 5. Friedman, S.L., Neuschwander-Tetri, B.A., Rinella, M. & Sanyal, A.J. Mechanisms of NAFLD
621 development and therapeutic strategies. *Nat Med* **24**, 908-922 (2018).
- 622 6. El-Serag, H.B. & Kanwal, F. Epidemiology of hepatocellular carcinoma in the United States:
623 where are we? Where do we go? *Hepatology* **60**, 1767-1775 (2014).
- 624 7. Torre, L.A., *et al.* Global cancer statistics, 2012. *CA Cancer J Clin* **65**, 87-108 (2015).
- 625 8. <http://www.who.int>. *Cancer* (2017).
- 626 9. Collaborators, G.B.D.O., *et al.* Health Effects of Overweight and Obesity in 195 Countries over
627 25 Years. *N Engl J Med* **377**, 13-27 (2017).
- 628 10. Ringelhan, M., Pfister, D., O'Connor, T., Pikarsky, E. & Heikenwalder, M. The immunology of
629 hepatocellular carcinoma. *Nat Immunol* **19**, 222-232 (2018).
- 630 11. Wolf, M.J., *et al.* Metabolic activation of intrahepatic CD8+ T cells and NKT cells causes
631 nonalcoholic steatohepatitis and liver cancer via cross-talk with hepatocytes. *Cancer Cell* **26**,
632 549-564 (2014).
- 633 12. Michelson, A.D. How platelets work: platelet function and dysfunction. *J Thromb*
634 *Thrombolysis* **16**, 7-12 (2003).
- 635 13. Chauhan, A., Adams, D.H., Watson, S.P. & Lalor, P.F. Platelets: No longer bystanders in liver
636 disease. *Hepatology* **64**, 1774-1784 (2016).
- 637 14. Gawaz, M., Langer, H. & May, A.E. Platelets in inflammation and atherogenesis. *J Clin Invest*
638 **115**, 3378-3384 (2005).
- 639 15. Jackson, S.P. Arterial thrombosis--insidious, unpredictable and deadly. *Nat Med* **17**, 1423-
640 1436 (2011).
- 641 16. Fujita, K., *et al.* Effectiveness of antiplatelet drugs against experimental non-alcoholic fatty
642 liver disease. *Gut* **57**, 1583-1591 (2008).
- 643 17. Lang, P.A., *et al.* Aggravation of viral hepatitis by platelet-derived serotonin. *Nat Med* **14**,
644 756-761 (2008).
- 645 18. Iannacone, M., *et al.* Platelets mediate cytotoxic T lymphocyte-induced liver damage. *Nat*
646 *Med* **11**, 1167-1169 (2005).
- 647 19. Iannacone, M., Sitia, G., Narvaiza, I., Ruggeri, Z.M. & Guidotti, L.G. Antiplatelet drug therapy
648 moderates immune-mediated liver disease and inhibits viral clearance in mice infected with
649 a replication-deficient adenovirus. *Clin Vaccine Immunol* **14**, 1532-1535 (2007).
- 650 20. Sitia, G., *et al.* Antiplatelet therapy prevents hepatocellular carcinoma and improves survival
651 in a mouse model of chronic hepatitis B. *Proc Natl Acad Sci U S A* **109**, E2165-2172 (2012).
- 652 21. Shen, H., Shahzad, G., Jawairia, M., Bostick, R.M. & Mustacchia, P. Association between
653 aspirin use and the prevalence of nonalcoholic fatty liver disease: a cross-sectional study
654 from the Third National Health and Nutrition Examination Survey. *Aliment Pharmacol Ther*
655 **40**, 1066-1073 (2014).
- 656 22. Musso, G., Cassader, M., Rosina, F. & Gambino, R. Impact of current treatments on liver
657 disease, glucose metabolism and cardiovascular risk in non-alcoholic fatty liver disease
658 (NAFLD): a systematic review and meta-analysis of randomised trials. *Diabetologia* **55**, 885-
659 904 (2012).
- 660 23. Wong, V.W., *et al.* Pathogenesis and novel treatment options for non-alcoholic
661 steatohepatitis. *Lancet Gastroenterol Hepatol* **1**, 56-67 (2016).

- 662 24. Clapper, J.R., *et al.* Diet-induced mouse model of fatty liver disease and nonalcoholic
663 steatohepatitis reflecting clinical disease progression and methods of assessment. *Am J*
664 *Physiol Gastrointest Liver Physiol* **305**, G483-495 (2013).
- 665 25. Wang, B., *et al.* Intestinal Phospholipid Remodeling Is Required for Dietary-Lipid Uptake and
666 Survival on a High-Fat Diet. *Cell Metab* **23**, 492-504 (2016).
- 667 26. Weston, C.J., *et al.* Vascular adhesion protein-1 promotes liver inflammation and drives
668 hepatic fibrosis. *J Clin Invest* **125**, 501-520 (2015).
- 669 27. Gomes, A.L., *et al.* Metabolic Inflammation-Associated IL-17A Causes Non-alcoholic
670 Steatohepatitis and Hepatocellular Carcinoma. *Cancer Cell* **30**, 161-175 (2016).
- 671 28. Angulo, P., *et al.* Liver Fibrosis, but No Other Histologic Features, Is Associated With Long-
672 term Outcomes of Patients With Nonalcoholic Fatty Liver Disease. *Gastroenterology* **149**,
673 389-397 e310 (2015).
- 674 29. Dulai, P.S., *et al.* Increased risk of mortality by fibrosis stage in nonalcoholic fatty liver
675 disease: Systematic review and meta-analysis. *Hepatology* **65**, 1557-1565 (2017).
- 676 30. Bayindir-Buchhalter, I., *et al.* Cited4 is a sex-biased mediator of the antidiabetic glitazone
677 response in adipocyte progenitors. *EMBO Mol Med* **10**(2018).
- 678 31. Mauri, L., *et al.* Twelve or 30 months of dual antiplatelet therapy after drug-eluting stents. *N*
679 *Engl J Med* **371**, 2155-2166 (2014).
- 680 32. He, G. & Karin, M. NF-kappaB and STAT3 - key players in liver inflammation and cancer. *Cell*
681 *Res* **21**, 159-168 (2011).
- 682 33. Kral, J.B., Schrottmair, W.C., Salzmann, M. & Assinger, A. Platelet Interaction with Innate
683 Immune Cells. *Transfus Med Hemother* **43**, 78-88 (2016).
- 684 34. Husted, S. & van Giezen, J.J. Ticagrelor: the first reversibly binding oral P2Y12 receptor
685 antagonist. *Cardiovasc Ther* **27**, 259-274 (2009).
- 686 35. Wallentin, L., *et al.* Ticagrelor versus clopidogrel in patients with acute coronary syndromes.
687 *N Engl J Med* **361**, 1045-1057 (2009).
- 688 36. Deppermann, C., *et al.* Gray platelet syndrome and defective thrombo-inflammation in
689 Nbeal2-deficient mice. *J Clin Invest* (2013).
- 690 37. Albers, C.A., *et al.* Exome sequencing identifies NBEAL2 as the causative gene for gray
691 platelet syndrome. *Nat Genet* **43**, 735-737 (2011).
- 692 38. Kahr, W.H., *et al.* Mutations in NBEAL2, encoding a BEACH protein, cause gray platelet
693 syndrome. *Nat Genet* **43**, 738-740 (2011).
- 694 39. Gunay-Aygun, M., *et al.* NBEAL2 is mutated in gray platelet syndrome and is required for
695 biogenesis of platelet alpha-granules. *Nat Genet* **43**, 732-734 (2011).
- 696 40. Kopec, A.K., *et al.* Thrombin promotes diet-induced obesity through fibrin-driven
697 inflammation. *J Clin Invest* **127**, 3152-3166 (2017).
- 698 41. Jandrot-Perrus, M., *et al.* Cloning, characterization, and functional studies of human and
699 mouse glycoprotein VI: a platelet-specific collagen receptor from the immunoglobulin
700 superfamily. *Blood* **96**, 1798-1807 (2000).
- 701 42. Drescher, H.K., *et al.* beta7-Integrin and MADCAM-1 play opposing roles during the
702 development of non-alcoholic steatohepatitis. *J Hepatol* **66**, 1251-1264 (2017).
- 703 43. Haemmerle, M., Stone, R.L., Menter, D.G., Afshar-Kharghan, V. & Sood, A.K. The Platelet
704 Lifeline to Cancer: Challenges and Opportunities. *Cancer Cell* **33**, 965-983 (2018).
- 705 44. Kleinschnitz, C., *et al.* Targeting platelets in acute experimental stroke: impact of
706 glycoprotein Ib, VI, and IIb/IIIa blockade on infarct size, functional outcome, and intracranial
707 bleeding. *Circulation* **115**, 2323-2330 (2007).
- 708 45. Kanaji, T., Russell, S. & Ware, J. Amelioration of the macrothrombocytopenia associated with
709 the murine Bernard-Soulier syndrome. *Blood* **100**, 2102-2107 (2002).
- 710 46. Subramaniam, M., *et al.* Defects in hemostasis in P-selectin-deficient mice. *Blood* **87**, 1238-
711 1242 (1996).
- 712 47. Blenner, M.A., Dong, X. & Springer, T.A. Structural basis of regulation of von Willebrand
713 factor binding to glycoprotein Ib. *J Biol Chem* **289**, 5565-5579 (2014).

- 714 48. Wang, Y., *et al.* Leukocyte integrin Mac-1 regulates thrombosis via interaction with platelet
715 GPIIb/IIIa. *Nat Commun* **8**, 15559 (2017).
- 716 49. George, J.N. Platelets. *Lancet* **355**, 1531-1539 (2000).
- 717 50. Langer, H.F., *et al.* Platelets contribute to the pathogenesis of experimental autoimmune
718 encephalomyelitis. *Circ Res* **110**, 1202-1210 (2012).
- 719 51. Romo, G.M., *et al.* The glycoprotein Ib-IX-V complex is a platelet counterreceptor for P-
720 selectin. *J Exp Med* **190**, 803-814 (1999).
- 721 52. Kroll, M.H., Harris, T.S., Moake, J.L., Handin, R.I. & Schafer, A.I. von Willebrand factor binding
722 to platelet GpIb initiates signals for platelet activation. *J Clin Invest* **88**, 1568-1573 (1991).
- 723 53. Wong, J., *et al.* A minimal role for selectins in the recruitment of leukocytes into the inflamed
724 liver microvasculature. *J Clin Invest* **99**, 2782-2790 (1997).
- 725 54. Dutting, S., *et al.* A Cdc42/RhoA regulatory circuit downstream of glycoprotein Ib guides
726 transendothelial platelet biogenesis. *Nat Commun* **8**, 15838 (2017).
- 727 55. Min, H.K., *et al.* Increased hepatic synthesis and dysregulation of cholesterol metabolism is
728 associated with the severity of nonalcoholic fatty liver disease. *Cell Metab* **15**, 665-674
729 (2012).
- 730 56. Townsend, S.A. & Newsome, P.N. Non-alcoholic fatty liver disease in 2016. *Br Med Bull* **119**,
731 143-156 (2016).
- 732 57. Neuschwander-Tetri, B.A., *et al.* Farnesoid X nuclear receptor ligand obeticholic acid for non-
733 cirrhotic, non-alcoholic steatohepatitis (FLINT): a multicentre, randomised, placebo-
734 controlled trial. *Lancet* **385**, 956-965 (2015).
- 735 58. Boege, Y., *et al.* A Dual Role of Caspase-8 in Triggering and Sensing Proliferation-Associated
736 DNA Damage, a Key Determinant of Liver Cancer Development. *Cancer Cell* **32**, 342-359 e310
737 (2017).
- 738 59. Franchi, F., Rollini, F. & Angiolillo, D.J. Antithrombotic therapy for patients with STEMI
739 undergoing primary PCI. *Nat Rev Cardiol* **14**, 361-379 (2017).
- 740 60. Margetts, J., *et al.* Neutrophils: driving progression and poor prognosis in hepatocellular
741 carcinoma? *Br J Cancer* **118**, 248-257 (2018).
- 742
- 743

744 **METHODS**

745 Methods, including statements of data availability and any associated accession
746 codes and references are available in the online version of the paper.

747

748 **Mice, diets and treatments**

749 4- to 5-week-old mice (C57BL/6J01aHsd) were purchased from ENVIGO. P-selectin
750 knockout mice (*Selep^{-/-}*) were purchased from Jackson Laboratories (mouse strain 002289).
751 Knockout mice for Nbeal2^{-/-}, GPVI (*Gp6^{-/-}*)⁶¹, GPIIb/IIIa (*GpIIB^{-/-}; Itga2b^{-/-}*), von Willebrand
752 factor (*vWF^{-/-}*) and also transgenic mice, lacking functional GPIb α , hIL4 α /GPIb α -Tg, all on
753 the background of C57Bl/6J were kindly provided by Professor Bernhard Nieswandt and
754 Prof. Jerry Ware (University Hospital and Rudolf Virchow Center, University of Würzburg,
755 Würzburg, Germany; Department of Physiology and Biophysics, University of Arkansas for
756 Medical Sciences, 4301 West Markham Street, Little Rock, Arkansas 72205, USA).
757 Inducible knock-in mice expressing the human unconventional prefoldin RPB5 interactor
758 (URI) in hepatocytes (hURI-tetOFFhep) were received from Prof. Dr. Nabil Djouder, CNIO,
759 Madrid. *Pdpnfl/flx Vav1-iCre* mice (obtained from Jackson Laboratories) and *Clec1bfl/flx Pf4-*
760 *Cre* mice are described elsewhere⁶². All strains of genetically-altered mice were on a
761 C57BL/6J background. Control mice were negative for cre recombinase and matched by
762 genetic background, age and sex. Mice were housed at the University Hospital Zurich (USZ),
763 the Technical University Munich/Helmholtz Zentrum Munich, the Biomedical Services Unit at
764 University of Birmingham or University of Newcastle, the University of Calgary and the
765 German Cancer Research Center (DKFZ). All animal work was conducted under the
766 approval of the Swiss Veterinary Office (136/2014), according to German Law (G7/17 or
767 55.2-1-54-2532-39-2015), the UK Animals Scientific Procedures Act of 1986, with project
768 licence approval granted by the UK Home Office, the local biomedical research ethics
769 committee approval and the University of Calgary Animal Care Committee (protocol AC16-
770 0148) in accordance with the Canadian Council for Animal Care Guidelines. Animals were
771 maintained under specific pathogen-free conditions and experiments were performed in

772 accordance to the guidelines of the respective institution and were in accordance with ethical
773 regulations and humane endpoints.

774 Five-week-old mice were fed *ad libitum*: normal diet (ND) (Provimi Kliba) or choline-deficient
775 high-fat diet (CD-HFD) (Research Diets; D05010402) for 6 or 12 months; Western diet with
776 trans-fat (WD-HTF) (Research Diets; D09100301 - 40 kcal % fat (Primex shortening), 20 kcal
777 % fructose, 2% cholesterol) for 6 months; methionine-choline-deficient diet (MCD) (MP
778 Biomedicals) for 4 weeks and control mice were fed a calorifically matched control diet;
779 Western diet with fructose in drinking water (WD-FSDW) (Custom Research Diet TD.06303;
780 Harlan Laboratories in conjunction with fructose-supplemented drinking water - 55% fructose,
781 45% glucose by weight at a concentration of 42 g/l *ad libitum* for 6 and 9 months. Control
782 animals received ND and non-supplemented drinking water.

783

784 Cohorts of mice fed CD-HFD or WD-HTF were in addition treated with either Aspirin (through
785 food pellets containing 7.5 mg per kg of food) in combination with Clopidrogel high (40 µg/ml
786 drinking water; ~3 mg/kg/day) or low dose (20 µg/ml drinking water; ~1.5 mg/kg/day), with
787 Sulindac (200 µg/ml drinking water; ~20 mg/kg/day) or with Ticagrelor (40 µg/ ml drinking
788 water; ~3 mg/kg/day).

789

790 For interventional studies five-week-old male mice were fed normal diet (ND) or choline-
791 deficient high-fat diet (CD-HFD) (Research Diets; D05010402) or Western Diet containing
792 trans-fat (WD-HTF) (Research Diets, D09100301) for 3.5 weeks and then treatment started
793 for 2.5 weeks, 2x per week i.v. in 100 µl PBS of either 20µg/mouse anti-CD44 antibody
794 (clone KM81, Cedarlane), 100 µg/mouse anti-CD44 (clone IM7, Bioxcell), 100µl/mouse
795 Clodrosome® (Liposomal Clodronate), 100µl/mouse Encapsome® (Control Liposomes),
796 100µg/mouse anti-GPIIbα or 100 µg/mouse Fab-Rat IgG (kindly provided by Prof. Bernhard
797 Nieswandt - University Hospital and Rudolf Virchow Center, University of Würzburg,
798 Würzburg, Germany) or i.p 20 U/gr murine hyaluronidase (HYAL). In late treatment regimes,

799 mice were fed CD-HFD for 6 months and treated with the same protocol for indicated time
800 points.

801 For osmotic Pump experiment five-week-old male mice were fed choline deficient high fat
802 diet (CD-HFD) (Research Diets; D05010402) for 12 weeks. 4 weeks after the diet (Mini-
803 pumps (Alzet, model 2004) were implanted subcutaneously into the mice to deliver 30 µg per
804 day of Ly6G (clone 1A8) neutrophil depleting antibody or Rat IgG2a (clone 2A3) (BioXCell)
805 for a further 8 weeks. At the end of the experiment, animals were culled, and the liver, fat and
806 serum harvested for analysis.

807

808 **Human material**

809 Specimens were obtained from formalin-fixed, paraffin-embedded non-diseased, NAFLD, or
810 NASH diagnosed human liver tissue, retrieved from the archives and the biobank of the
811 Department of Pathology and Molecular Pathology, University Hospital Zurich, University
812 Hospital Würzburg and in the setting of the HEP-CAR consortium (Institute for Research in
813 Biomedicine (IRB) Barcelona). Tissues were examined by certified liver pathologists (Prof.
814 Prof. Achim Weber, Prof. Josep M. Llovet.). These studies were approved by the local ethics
815 committee ("Kantonale Ethikkommission Zürich", application numbers StV26/2005 and KEK-
816 ZH-Nr. 2013-0382) or the Institute for Research in Biomedicine (IRB) Barcelona, Hospital
817 Clinic HCB/2015/0789. In line with the regulation of KEK, individual informed consent from all
818 patients was not required for this kind of retrospective analysis on patients' material.

819

820 The prospective clinical trial has been listed at the German Clinical Trials Register (DRKS),
821 evaluated and accepted by the local ethical authorities (Ethik-Kommission
822 Universitätsklinikum Tübingen) with the Nr.587/2016BO2 - under the name: "Platelet
823 inhibition to recues formation of non-alcoholic steatohepatitis in cardiovascular patients"
824 (Prometheus - prospective, monocenter, observational study).

825

826

827

828

829 **Prospective trial, ethics, MRI and ultrasound analyses**

830 The case study of 24 individual observations prospective trial was approved by the
831 institutional ethics committee (587/2016BO2) and comply with the declaration of Helsinki and
832 the good clinical practice guidelines⁶³⁻⁶⁶.

833 For the prospective, ongoing case study, we have included only patients (n=23) with
834 diabetes mellitus type II and/or BMI>30, two risk factors, that are highly correlated with
835 development of NAFLD/NASH. All patients underwent cardiac catheterization due to
836 suspected coronary artery disease (CAD). Patients received no antiplatelet treatment if CAD
837 was excluded. Patients received antiplatelet therapy with 100mg acetylsalicylic acid (ASA)
838 once daily if CAD was present but coronary stent implantation was not indicated. Patients
839 received dual antiplatelet therapy with ASA 100 mg once daily and P2Y12 inhibitor
840 (Clopidogrel 75mg once daily, Ticagrelor 90mg twice daily or Prasugrel 10mg once daily)
841 depending on acuity and severity of CAD (e.g. myocardial infarction vs. stable CAD). None of
842 the patients included received long-term treatment with ASA or P2Y12 before study
843 inclusion.

844

845 All patients remained on the respective treatment regimens until time point of follow-up. All
846 patients underwent liver MRI and liver ultrasound at baseline (within 4 weeks after hospital
847 discharge) and after 6 months of follow up. The serum from all patients was analyzed for
848 classic liver damage parameters like AST, ALT, Bilirubin, GGT etc. Additional measurements
849 were performed to exclude other than NAFLD reasons for liver damage, e.g. immune-
850 hepatitis, viral hepatitis, AFLD. All patients underwent the Michigan Alcoholism Screening
851 Test to evaluate drinking habits. Patients with left ventricular ejection fraction <45% or severe
852 valve diseases were not included into the study due to the risk of liver congestion.

853 The hepatic lipid accumulation was quantified by 3 T MRI (Skyra, Siemens Healthcare,
854 Erlangen Germany) at the Department of Diagnostic and Interventional Radiology of the
855 University Hospital of Tübingen, Germany. A commercially available multi-echo Dixon
856 sequence (LiverLab, Siemens Healthcare, Erlangen Germany) was used, allowing the
857 computation of proton density fat fraction maps and inline segmentation of the liver.
858 Ultrasound examinations in patients were performed twice, at the time point of patient
859 recruitment and six months after patient recruitment. In order to identify patients presenting
860 with signs of liver steatosis or with signs of liver cirrhosis, bright hepatic echos, increased
861 hepatorenal echogenicity, presence of nodular liver morphology and signs of portal
862 hypertension (e.g. splenomegaly, ascites or intra-abdominal varices) were analyzed using an
863 Aplio 500/T1 (Toshiba) / Ultrasonic transducer 3-5 MHz.

864

865 The multivariate analysis (age, gender, antiaggregation and new statin treatment) to identify
866 statin administration as a possible confounder of the observed effects, patients were
867 differentiated into groups, that received statin treatment prior to hospital admission and those
868 that received new statin treatment at hospital discharge prior to the first MRI examination.

869 We performed a linear regression analysis.

870 [For further details regarding the human samples, please refer to the Supplementary Material](#)
871 [\(Table 1a, Table 1b, Table 2\).](#)

872

873 **Cholesterol measurements**

874 Hyperlipidemia is defined as baseline LDL cholesterol ≥ 160 mg/dl and triglycerides ≥ 200
875 mg/dl. Interestingly, only 3 of the patients of the prospective cohort offer triglyceride values
876 ≥ 200 mg/dl. However, all patients of the prospective cohort show significantly elevated liver
877 fat accumulation indicating that patients might not need elevated serum lipid levels to
878 develop fatty liver disease. As previously mentioned, according to our measurements, only 3
879 patients of the prospective trial fulfill the diagnosis hyperlipidemia. However, we decided to
880 stay with pre-existing conditions e.g. diagnosed by family doctors because serum lipid levels

881 undergo dynamic regulations. This explains the discrepancy between hyperlipidemia and
882 measured lipid levels in baseline Table 2.

883

884 **Isolation of liver leukocytes for in depth myeloid characterization**

885 Livers were perfused once with PBS followed by collagenase digestion at 37°C for 40
886 minutes (collagenase type IV, Worthington, UK). Additionally, 0.1 mg/ml DNase I was added
887 after 20 min. Single cell suspension was obtained by filtering the digested liver through a 70
888 µm mesh. Hepatocytes were removed by low speed centrifugation (50 rcf, 1 min) and density
889 gradient centrifugation was performed using 18 % Nycodenz dissolved in Gey's Balanced
890 Salt Solution (GBSS) as previously described.⁶⁷

891

892 Cells were then stained for CD206 (C068C2), CX3CR1 (SA011F11), CD3 (17A2), MHC-II
893 (M5/114.15.2) (all Biolegend); CD11b (M1/70), F4/80 (BM8) (all Invitrogen); CD86 (GL-1,
894 eBioscience); CD45 (30-F11), Ly6C (RB6-8C5), Ly6C (1A8) CD11c (HL3), CD31 (MEC13.3),
895 NK1.1 (PK136), TIM-4 (RMT4-54) (all BD Bioscience) followed by multi-color flow cytometry
896 using an LSR-Fortessa (BD Biosciences). Analysis was done using FlowLogic (v7.2, Inivai,
897 Australia) and FlowJo (v10.4, BD Biosciences). Additionally, liver MoMF and KC for
898 NanoString gene expression analysis were sorted using an Aria-II (BD Biosciences).

899 **For the details regarding the definition of violin-plot elements of Supplemental Figure 3i,**
900 **please, refer to the Supplementary Material (Table 3).**

901

902 **t-distributed stochastic neighbor embedding (t-SNE)**

903 Liver leukocytes were pre-gated for living (7-AAD-), CD45+, Ly6G-, CD31-, F4/80+ cells by
904 using FlowJo (v10.4, BD Biosciences), followed by t-SNE based clustering as described
905 previously,⁶⁸ by using the Rtsne package for R. Clusters were identified by hierarchical
906 clustering and projected onto the two dimensional t-SNE plot, while relative protein
907 expression was displayed for each cluster by violin plots using R (v3.5.1).

908

909 **nCounter gene expression analysis**

910 Gene expression analysis of 561 selected gene targets of liver MoMF and KC was done by
911 using NanoString assays (nCounter Mouse Immunology Kit, NanoString Technologies).
912 Analysis was done by using the nSolver Software (v2.0, NanoString Technologies). Principal
913 component analysis (PCA) was done by using the prcomp package for R (v3.5.1).

914

915 **Measurement of serum parameters**

916 Serum was isolated from mice and liver enzymes AST and ALT were quantified by Roche
917 Modular System (Roche Diagnostics) with a commercially available automated colorimetric
918 system at the Institute of Clinical Chemistry at the University Hospital Zurich using a Hitachi
919 P-Modul (Roche). Total cholesterol was measured in a 96-well format using CHOL or TG
920 GPO-PAP substrates (Roche Diagnostics).

921

922 **Measurement of liver triglycerides**

923

924 Liver specific triglyceride levels were analyzed from snap-frozen liver tissue samples. Liver
925 tissue samples were homogenized in sodium chloride (0.9 % NaCl) and liver resident lipids
926 were precipitated using ethanolic potassium hydroxide (0.5 M KOH) and solubilized in
927 magnesium sulphate (0.15 M MgSO₄). The concentration of hepatic triglycerides was then
928 measured using triglycerides GPO-PAP from Roche Diagnostics on a spectrophotometer at
929 505 nm.

930

931 **Intraperitoneal glucose tolerance test**

932 Intraperitoneal glucose tolerance tests (IPGTTs) were carried out on mice fasted overnight
933 for 16 h. Basal blood glucose concentrations were determined for each mouse prior to
934 glucose (2 mg/g body weight) administration using a hand-held glucose analyzer (FreeStyle
935 Freedom Lite; Abbott). Each mouse then received glucose via intraperitoneal (i.p.) injection
936 and blood glucose concentrations were subsequently re-measured 15, 30, 60 and 120 min
937 post glucose administration.

938

939

940

941 **Intraperitoneal insulin tolerance test and fasting insulin determination**

942 Intraperitoneal insulin tolerance tests were carried out on mice mild fasted for 6 h. Basal
943 blood glucose concentrations were determined for each mouse prior to insulin (1U/g lean
944 mass determined by EchoMRI analysis) administration using a hand-held glucose analyzer
945 (FreeStyle Freedom Lite; Abbott). Each mouse then received Insulin via intraperitoneal (i.p.)
946 injection and blood glucose concentrations were subsequently re-measured 15, 30, 60 and
947 120 min post glucose administration. Fasted insulin levels were measured in mildly fasted
948 (8h) using ALPCO mouse insulin ELISA kit.

949

950 **Immunoblot analysis**

951 Liver homogenates were prepared in a pH 7.4 lysis buffer containing 1% NP-40 (Sigma-
952 Aldrich, Gillingham, UK), 50 mmol/L Tris, 10% glycerol, 0.02% NaN₃, 150 mmol/L NaCl, and
953 a cocktail of phosphatase and protease inhibitors (Sigma-Aldrich, Gillingham, UK), and
954 protein concentration was determined using the Pierce BCA Protein Assay Kit (Thermo
955 Scientific) according to the manufacturer's manual. Liver homogenates were prepared using
956 a homogenizer. Tissue preparation was performed with gentleMACS™ Octo Dissociator
957 (Miltenyi Biotec GmbH). 20–80 µg of proteins were separated under reducing conditions
958 (2.5% β-mercaptoethanol) by gel electrophoresis (Mini Protean Gels, Bio Rad) and blotted by
959 semi-dry blotting (Trans-Blot Turbo Transfer, Bio Rad) onto nitrocellulose membranes (Bio
960 Rad). Membranes were blocked in 5% milk/PBS-T for at least 1 hr at RT. Primary antibodies
961 against P-p38MAPK ((Thr180/Tyr182) D3F9), p38 MAPK (D13E1), P-p65 (Ser536), p65
962 (D14E12), COX1 (D5H5), GAPDH (14C10) (all Cell Signaling) were incubated at 4°C
963 overnight under shaking conditions. Incubation with the secondary antibody (HRP-anti rabbit
964 IgG, 1:5000; Promega) was performed under shaking conditions for 1 hr. Detection was

965 achieved using Clarity Western ECL Substrate (Bio Rad) using Stella 3200 imaging system
966 (Raytech).

967

968

969 **Flow cytometry**

970 For flow cytometry analysis, antibodies against CD8- α (53-6.7), CD3- ϵ (500A2), IgM (RMM-
971 1), CD19 (6D5), NK1.1 (PK136), were purchased from BioLegend. Antibodies against CD4
972 (RM4-5) and Foxp3 (FJK-16s) were purchased from eBioscience. Viability was assessed by
973 LIVE/DEAD Fixable Aqua or ZombieDyeNIR (Life Technologies). TA99 was labeled with an
974 Alexa Fluor 647 NHS Ester (Life Technologies) to generate TA99-647. Further antibodies
975 that were used include CD44: Clone IM7, Biolegend, diluted 1:200, CD69: Clone H1.2F3,
976 Biolegend, diluted 1:200, CD62L: Clone MEL-14, Biolegend, diluted 1:200. Intracellular
977 cytokine staining (ICS) was performed as described previously¹¹. Peptides used for
978 restimulation were 10 μ g/ml of the relevant antigen: Trp2180-188 (SVYDFFVWL),
979 Her2/Neu66-74 (TYVPANASL), Tyrp-1455-463native (TAPDNLGYA), or gp10025-33native
980 (EGSRNQDWL). Cells were analyzed using BD FACS LSR II, BD FACS LSR Fortessa, BD
981 FACSCanto, Sony spectral analyzer SP6800 flow cytometers, and data were analyzed using
982 FlowJo.

983

984 **Histology, immunohistochemistry, scanning and automated analysis**

985 Liver samples were fixed in 4% paraformaldehyde and paraffin-embedded at the University
986 Hospital Zürich, Department of Pathology and Molecular Pathology Core, at the Technical
987 University of Munich (TUM), or at the DKFZ, Department of Chronic Inflammation and
988 Cancer (Heidelberg) as described¹¹. Briefly, 2 μ m sections from FFPE and cryo-preserved
989 tissues were prepared and stained with Hematoxylin/Eosin or IHC antibodies. Incubation in
990 Ventana buffer and staining was performed on a NEXES immunohistochemistry robot
991 (Ventana Instruments) using an IVIEW DAB Detection Kit (Ventana) or on a Bond MAX
992 (Leica). For Sudan Red staining, cryo sections (5 μ m) were cut and stained with Sudan Red

993 (0.25% Sudan IV in ethanolic solution). Slides were scanned with a Nano Zoomer
994 (Hamamatsu, Japan).

995

996 Antibodies that were used include: anti-MHCII, rat (clone M5/114.15.2) 1:500, anti-CD3,
997 rabbit (clone SP7) 1:250, anti-F4/80, rat, BioLegend Cat# 123105; 1:50. Further antibodies
998 used include: Collagen IV, rabbit 1:50, Cedarlane, clone CL50451AP-1; Ki67, rabbit 1:200,
999 Thermo Scientific, clone RM-9106-S1; B220, rat 1:3000, BD, clone 553084; Ly6G rat 1:600,
1000 BD, clone 551459, PERK1/2, rabbit, 1:400, Cell Signaling, clone 4370; Glutamine
1001 Synthetase (GS) rabbit 1:500, abcam, clone ab16802, PSTAT3, rabbit, 1:100, Cell signaling
1002 clone 9145.

1003

1004 For quantification of stains, slides were scanned using a SCN400 slide scanner (Leica) and
1005 analyzed using Tissue IA image analysis software (4.0.6 Slidepath, Leica). For quantification
1006 of platelet staining on human (CD61) and mouse (CD42b) tissue software based analysis
1007 and counting at the screen (CD42b; 100 high-power fields; 40x) was performed.

1008 For Sudan Red⁺ liver area, data are presented as Sudan Red positive area in percent of total
1009 tissue area. Three random liver tissue areas of approximately 6-8 mm² (87000 μm²) were
1010 selected in DIH (digital image hub, Leica), submitted to analysis and merged.

1011 NASH activity score (NAS) was applied to murine livers.

1012

1013 **Electron microscopy**

1014 For electron microscopy, sections from epon-embedded, glutaraldehyde-fixed liver samples
1015 were cut and stained with toluidine blue. The tissue was trimmed and ultrathin cross sections
1016 of the liver were cut and treated with uranyl acetate and lead citrate as described
1017 previously⁶⁹. Electron micrographs were analyzed for cell composition and localization using
1018 the analySIS Docu System (Soft Imaging System GmbH).

1019

1020 **Preparation of mouse platelets**

1021

1022 Blood was obtained from the tail of mice and was drawn into citrate tubes at a 1:10 ratio.
1023 Platelet-rich plasma (PRP) was obtained by centrifugation at 260 g for 5 minutes. Afterward,
1024 platelet-rich plasma was centrifuged at 640 g for 5 minutes to pellet the platelets. After 2
1025 washing steps, the pellet of washed platelets was resuspended in modified Tyrode-HEPES
1026 buffer (pH 7.4, supplemented with 1mM CaCl₂).

1027

1028 **Platelet aggregometry**

1029 Washed platelets were adjusted to a concentration of 150x10³ platelets/μl in Tyrode-HEPES
1030 buffer (pH 7.4 supplemented with 1mM CaCl₂). Aggregation was estimated from light
1031 transmission determined with a luminoaggregometer model 700 (ChronoLog, Havertown,
1032 PA, USA). Following calibration, agonists including Adenosine 5'-diphosphate (ADP),
1033 U46619 (U46), thrombin (Thr), collagen-related peptide (CRP), rhodocytin (RC) were added
1034 at the indicated concentrations and aggregation was measured for 10 minutes with a stir
1035 speed of 1000 rpm at 37 °C. Afterwards analysis was performed using the aggroLink8
1036 software (ChronoLog).

1037

1038 **Analysis of platelets and flow cytometry of platelets**

1039

1040 Mice were bled under isoflurane anesthesia. Blood was collected in a tube containing 20
1041 U/ml heparin, and PRP was obtained by 2 cycles of centrifugation at 300 g for 6 min at room
1042 temperature (RT). For preparation of washed platelets, PRP was washed twice at 800 g for 5
1043 minutes at RT and the pellet was re-suspended in modified Tyrodes-HEPES (N-2-
1044 hydroxyethyl-piperazone-N'-2-ethanesulfonic acid) buffer (134 mM NaCl, 0.34 mM Na₂HPO₄,
1045 2.9 mM KCl, 12 mM NaHCO₃, 5 mM HEPES, 1 mM MgCl₂, 5 mM glucose, 0.35% BSA, pH
1046 7.4) in the presence of prostacyclin (0.1 μg/ml) and apyrase (0.02 U/ml).

1047 Apyrase grade III (Sigma-Aldrich), prostacyclin (PGI₂), ADP (Sigma-Aldrich), U-46619 (Enzo
1048 Life Sciences), thrombin (Roche), (Sigma-Aldrich), rabbit anti-human VWF (DAKO), rabbit
1049 anti-human fibrinogen (DAKO) were purchased as indicated. CRP and Rhodocytin were
1050 generated and isolated as previously described³⁶. The antibody against the activated form of

1051 integrin α IIb β 3 (JON/A-PE) was from Emfret Analytics. Other antibodies we received were
 1052 generated in the laboratory of Prof. Nieswandt as following:
 1053

Antibody	Clone	Isotype	Antigen	Reference
JON/A	4H5	IgG2b	α IIb β 3	70
WUG 1.9	5C8	IgG1	P-selectin	71
JAQ1	98A3	IgG2a	GPVI	72
LEN1	12C6	IgG2b	α 2	73
ULF1	96H10	IgG2a	CD9	74
p0p4	15E2	IgG2b	GPIb	74
p0p6	56F8	IgG2b	GPIX	74
JON2	14A3	IgG2b	α IIb β 3	74
DOM2	89H11	IgG2a	GPV	74
INU1	11E9	IgG1	CLEC-2	75

1054

1055 **RNA isolation and quantitative real-time PCR**

1056 Total RNA was isolated from snap-frozen liver tissues according to the manufacturer's
 1057 protocol using RNeasy Mini Kit (Qiagen). The quantity and quality of the RNA was
 1058 determined spectroscopically using a Nanodrop analyser (Thermo Scientific). 1 μ g of purified
 1059 RNA was subsequently transcribed into cDNA using Quantitect Reverse Transcription Kit
 1060 (Qiagen) according to the manufacturer's protocol. Quantitative RT-PCR was performed
 1061 using Fast Start SYBR Green Master Rox (Roche). Primers were custom made by
 1062 Microsynth as previously described¹¹. For mRNA expression analysis quantitative real-time
 1063 PCR was performed in duplicates in 384-well plates using Fast Start SYBR Green Master
 1064 Rox (Roche) on a 7900 HT qRT-PCR system (Applied Biosystems, Life Technologies
 1065 Darmstadt, Germany). Relative mRNA levels were calculated according to the $\Delta\Delta$ Ct relative

1066 quantification method and were normalized to a house-keeping gene (GAPDH or ROTH2)
1067 levels. The data were normalized to the expression of housekeeping gene and analyzed
1068 using the GraphPad Prism software version 7.03 (GraphPad Software). For the analysis of
1069 whole liver homogenates by microarray (Agilent) the following genes were selected,
1070 analyzed and shown. For a list of all used primers for RT-qPCRs please refer to
1071 Supplementary Material Table 4.

1072 **Gene expression profiling**

1073 Transcriptional profiling was performed using SurePrint G3 Mouse Gene Expression 8x60k
1074 microarrays (Agilent Technologies, AMADID 28005) according to the manufacturer's
1075 protocol. 75 ng of total RNA was used in labeling using the Low Input Quick Amp Labeling Kit
1076 (one-color, Agilent Technologies). Raw gene expression data were extracted as text files
1077 with the Feature Extraction software 11.0.1.1 (Agilent Technologies). The expression
1078 microarray data were uploaded to ArrayExpress (www.ebi.ac.uk/arrayexpress/) and the data
1079 set is available under the accession number E-MTAB-6073, entitled "Transcriptomic
1080 differences in livers of mice fed with normal diet and choline-deficient high-fat diet".

1081 All data analysis was conducted using the R statistical platform (version 3.2.2, [www.r-](http://www.r-project.org)
1082 project.org). Data quality assessment, filtering, preprocessing, normalization, batch
1083 correction based on nucleic acid labeling batches and data analyses were carried out with
1084 the Bioconductor R-packages limma, Agi4x44PreProcess and the ComBat function of the
1085 sva R-package. All quality control, filtering, preprocessing and normalization thresholds were
1086 set to the same values as suggested in Agi4x44PreProcess R-package user guide. Only
1087 HGNC annotated genes were used in the analysis. GSEA was conducted on calculated log₂-
1088 expression values of all array probes using the „GSEA Pre-ranked“ function with default
1089 settings⁷⁶.

1090

1091 **RNA sequencing**

1092 Library preparation for bulk 3'-sequencing of poly(A)-RNA was done as described
1093 previously⁷⁷. Briefly, barcoded cDNA of each sample was generated with a Maxima RT
1094 polymerase (Thermo Fisher) using oligo-dT primer containing barcodes, unique molecular
1095 identifiers (UMIs) and an adapter. 5' ends of the cDNAs were extended by a template switch
1096 oligo (TSO) and after pooling of all samples full-length cDNA was amplified with primers
1097 binding to the TSO-site and the adapter. cDNA was tagmented with the Nextera XT kit
1098 (Illumina) and 3'-end-fragments finally amplified using primers with Illumina P5 and P7
1099 overhangs. In comparison to Parekh S *et. al.* 2016, the P5 and P7 sites were exchanged to
1100 allow sequencing of the cDNA in read1 and barcodes and UMIs in read2 to achieve a better
1101 cluster recognition. The library was sequenced on a NextSeq 500 (Illumina) with 75 cycles
1102 for the cDNA in read1 and 16 cycles for the barcodes and UMIs in read2.

1103

1104 **RNASeq analysis**

1105 Gencode gene annotations version M18 and the mouse reference genome GRCm38.p6
1106 were derived from the Gencode homepage (<https://www.gencodegenes.org/>). Dropseq tools
1107 v1.12⁷⁸ was used for mapping the raw sequencing data to the reference genome. The
1108 resulting UMI filtered countmatrix was imported into R v3.4.4. Prior differential expression
1109 analysis with DESeq2 1.18.1⁷⁹, dispersion of the data was estimated with a parametric fit
1110 including the dietary status of the mice as explanatory variable in the model. The Wald test
1111 was used for determining differentially regulated genes between the high fat and normal diet
1112 group and shrunken log2 foldchanges were calculated afterwards with setting the type
1113 argument of the lfcShrink function to 'normal'. A gene was determined to be differentially
1114 regulated if the absolute log2 foldchange| was greater than 1 and the adjusted p-value was
1115 below 0.05. Gene set enrichment analysis was conducted with EnrichR⁸⁰ within the
1116 Reactome database. Raw sequencing data is available under the accession number MTAB-
1117 7625.

1118

1119 **MRI analysis for mice**

1120 Steatosis was analyzed in 6-month-old B6 mice fed with ND, CD-HFD or CD-HFD/Asp-Clop
1121 treated groups. A Pharmascan 7T MRI (Bruker) with Paravision 5.1 software was used in
1122 FLASH scan mode without fat suppression using an echo-time of 2.2 ms for out-phase and
1123 2.9 ms for in-phase based on previous reports^{81,82}.

1124

1125 **Calorimetric TSE analysis**

1126 Mice were individually housed for indirect calorimetry in PhenoMaster (TSE systems). Mice
1127 were allowed to acclimate to the new environment for at least 2-3 days followed by recording
1128 of metabolic parameters such as food and water intake, O₂ consumption, CO₂ production,
1129 respiratory exchange ratio and total activity. All parameters were measured for at least four
1130 consecutive days with 5 measurement values every hour. Analysis of covariance (ANCOVA)
1131 was first conducted to ensure that body weight does not play a significant effect on the
1132 measured parameters.

1133

1134 **Immunofluorescence microscopy of liver sections**

1135 To achieve rapid fixation after euthanasia, livers were fixed with paraformaldehyde–lysine–
1136 periodate (PLP) for 4–8 h, rehydrated in 30% sucrose solution for 48 h and snap frozen in
1137 OCT (Cell Path). Thick (5 µm) cryosections were obtained using a Leica Cryostat and the
1138 Cryojane tape transfer system (Leica Microsystems).

1139

1140 **Generation of liver slices for confocal microscopy**

1141 The generation of the liver slices for microscopy was performed and adapted from a
1142 previously described protocol⁸³. Briefly, livers were collected and processed as described
1143 above. OCT-embedded frozen livers were iteratively sectioned using a cryostat. Samples
1144 were then reversed and the procedure was repeated on the opposite face of the liver until a
1145 30 µm thick slice of liver was obtained. OCT freezing medium covering the sample was
1146 removed, and slices were washed with PBS and blocked overnight at 4 °C in blocking

1147 solution (0.2% Triton/1%BSA/10% donkey serum/PBS). Liver slices were stained with Rat
1148 anti-CD41, goat anti-CD105, rabbit anti-Col IV and rabbit anti-CD8 for 3 days in blocking
1149 solution, washed overnight in PBS and stained with DyLight488 donkey anti-rabbit IgG and
1150 DyLight549 or DyLight649 donkey anti-rat IgG. Stained slices were then washed in PBS and
1151 incubated overnight in FocusClear (CelExplorer Lab). For observation under the confocal
1152 microscope, liver slices were embedded in FocusClear and mounted on glass slides.

1153

1154 **Immunofluorescence staining**

1155 Livers were perfused with PBS trough inferior vena cava, harvested and fixed in 4%
1156 paraformaldehyde for 16 h, then dehydrated in 30% sucrose prior to embedding in OCT
1157 freezing media (Sakura). 25 micrometer sections were cut on a HM550 cryostat
1158 (ThermoFisher) and adhered to Superfrost Plus slides (Thermo Scientific). Sections were
1159 then permeabilized and blocked in PBS containing 0.3% Triton X-100 (Sigma-Aldrich) and
1160 10% FBS followed by staining in the same blocking buffer. The following primary Abs were
1161 used for staining: rabbit anti-collagen IV (1:200 Abcam-10808); CD41 PE (1:100 MWRReg-30
1162 Biologend), rat anti-F4/80 APC (1:100 BM8 thermofisher), rabbit ant-CD3 (1:100 DAKO
1163 A0445229-2), B220 AF 647 (1:100 RA3-6B2 Biologend), CD11b APC (1:100 M1/70
1164 Biologend). Stained slides were mounted with fluorescent mounting medium (DAKO) and
1165 images were acquired on an inverted Leica microscope (TCS STED CW SP5, Leica
1166 Microsystems) with a motorized stage for tiled imaging.

1167

1168 To minimize fluorophore spectral spillover, we used the Leica sequential laser excitation and
1169 detection modality. The bleed-through among sequential fluorophore emission was removed
1170 applying simple compensation correction algorithms to the acquired images. The
1171 semiautomatic surface-rendering module in Imaris (Bitplane) was used to create 3D
1172 volumetric surface objects corresponding either to individual cells or to the liver sinusoids.
1173 Signal thresholds were determined using the Imaris Surface Creation module, which

1174 provides automatic threshold identification and value-based visual surface thresholding
1175 around the positively stained objects.

1176

1177 For the semi-quantitative analysis of platelet adhesion to liver sinusoids, high resolution
1178 confocal xyz stacks of 30xy sections (1024 x 1024 pixel) sampled with 0,5 μm z spacing
1179 were acquired to provide image volumes of 388 x 388 x 30 μm^3 . The confocal z stacks were
1180 imported into Imaris software (Bitplane) and platelets were reconstructed as 3D volumes by
1181 means of the semiautomatic surface-rendering module with a seed point diameter of 2.08 μm
1182 (the mean platelet diameter^{84,85}). The split touching objects option of the module supports
1183 the separation of two or more objects that are identified as one, enabling the splitting of
1184 aggregates into single components. All analysis was performed at least on 12 random FOV.

1185

1186 **Confocal imaging analysis**

1187 For platelet aggregate size analysis, the surface and volume of each single platelet
1188 aggregate (containing more than 2 single platelet) from at least 12 different FOV was
1189 automatically obtain from the surface-rendering module (imaris, Bitplane); The
1190 PLT/endothelium coverage was derived from the same FOV as percentage of the total
1191 sinusoidal surface (calculated in each FOV) covered by PLT.

1192 For the quantification of the immune cells PLT interaction the number of immune cells (CD3⁺,
1193 CD11b⁺ and B220⁺) adjacent and non-adjacent to PLT (see supplementary movie S1 and
1194 S2) was manually counted in 12 FOV. The interaction was expressed as total number
1195 adjacent cell as well as percentage of cell adjacent to PLT over the total number of cells.

1196 The CD3⁺ cells/PLT interaction was further analyzed by calculating, for each cells, the
1197 contact surface area between them.

1198

1199

1200

1201

1202 **Multiplex ELISA**

1203 Cytokines and chemokines in whole liver of ND, CD-HFD and Asp-Clo treated CD-HFD mice
1204 (12 months old) were evaluated using a laser bead technology based Mouse Cytokine Array
1205 / Chemokine Array 31-Plex (MD31) by Eve Tech (Eve Technologies, Calgary, AB, Canada).

1206

1207 **Cytokine Profiler**

1208 Cytokines and chemokines in whole liver of ND, CD-HFD (ctrl ab) and CD-HFD (anti-GPIIb
1209 antibody) mice (6 months old) or in CD-HFD and CD-HFD/hIL4R α /GPIIb α -Tg mice (12
1210 months old) were assessed using the Mouse XL Cytokine Array Kit by R&D Systems.

1211

1212 **Spinning-disc microscopy**

1213 All imaging experiments were performed using 7 – 12 weeks old male mice. All mice were
1214 co-housed and bred in a specific pathogen-free facility at the University of Calgary with a 12
1215 hour light/dark cycle and access to food and water ad libitum.

1216

1217 **Preparation for intravital Microscopy**

1218 Multichannel spinning-disk confocal microscopy was used to image the liver as previously
1219 described (Surewaard and Kubes 2017). Briefly, mice were anesthetized by intraperitoneal
1220 injection of ketamine (200 mg/kg body weight; Bayer Animal Health) and xylazine (10 mg/kg
1221 body weight; Bimeda-MTC). A catheter was inserted into the tail vein to allow for
1222 administration of fluorescently conjugated antibodies, proteins and additional anesthetics. A
1223 midline and lateral abdominal incision were made, and the abdominal wall was partly
1224 removed to access the liver. The mouse was placed in a right lateral position on a heating
1225 plate to maintain body temperature at 37°C. The liver was exteriorized onto a glass coverslip
1226 and covered with moisturized laboratory tissues to restrict movement and breathing artefacts.
1227 Abdominal organs were covered with saline-soaked gauze to prevent dehydration.

1228

1229

1230 **Intravital microscopy**

1231 Image acquisition of the liver was performed using an inverted spinning-disk confocal
1232 microscope (IX81; Olympus), equipped with a focus drive (Olympus) and a motorized stage
1233 (Applied Scientific Instrumentation). The microscope was fitted with a motorized objective
1234 turret equipped with 43/0.16 UPLANSAPO, 103/0.40 UPLANSAPO, and 203/0.70
1235 UPLANSAPO objective lenses. The microscope was linked with a confocal light path
1236 (WaveFx; Quorum Technologies) based on a modified CSU-10 head (Yokogawa Electric
1237 Corporation). Cells of interest were visualized using fluorescently conjugated antibodies.
1238 Volocity software (Perkin Elmer) was used to drive the confocal microscope and for
1239 acquisition and analysis of images.

1240

1241 **Antibodies for intravital imaging**

1242 Antibodies for intravital imaging were as follows: Alexa Fluor (AF) 750–conjugated anti–
1243 mouse F4/80 (2 µg/mouse; clone BM8; AbLab), Alexa Fluor (AF) 647-conjugated anti-mouse
1244 CD49b (3 µg/mouse; clone HMa2; BioLegend), PE-conjugated anti-mouse Ly6G (3
1245 µg/mouse; clone 1A8; BioLegend) and FITC-conjugated anti-mouse CD3e (2µg(mouse;
1246 clone 145-2c11; eBioscience). HAPB (Sigma Aldrich) was fluorescently (Alexa Fluor 555;
1247 Invitrogen) conjugated and injected intravenously to detect intrahepatic HA.

1248

1249

1250 **In vivo treatments**

1251 Kupffer cell depletion was performed by intravenous injection of 100µl Clodronate (17 mM)
1252 i.v. twice a week for two weeks. Hyaluronidase (Sigma-Aldrich) was given by intraperitoneal
1253 injection twice a week at a dose of 20U/g per mouse for two weeks. The last dose was given
1254 3 hours before intravital imaging.

1255

1256

1257

1258 **In vivo image analysis**

1259 All videos and images were acquired and processed using Volocity software (PerkinElmer).
1260 Quantification of platelet aggregation, Kupffer cell and neutrophil numbers and sinusoid
1261 diameters was also performed using Volocity software. Per mouse, ten fields of view (FOV)
1262 were randomly selected and assessed. Platelet aggregation was measured using the “find
1263 objects” function in Volocity software and the highest background was subtracted as
1264 described (Surewaard et al 2018). Kupffer cell and neutrophil numbers were manually
1265 counted in ten randomly selected FOV. For measurement of sinusoidal diameter, images
1266 were exported from Volocity software as .jpg files. ImageJ software (NIH) was used to
1267 measure sinusoid diameters. Per mouse we measured 10 randomly selected sinusoids in 5
1268 fields of view (FOV).

1269

1270 **Statistical Analyses**

1271 Mouse data are presented as the mean \pm SEM. Pilot experiments and previous published
1272 results were used to estimate the sample size such that appropriate statistical tests could
1273 yield significant results. Statistical analysis was performed using GraphPad Prism software
1274 version 7.03 (GraphPad Software). Data of three or more groups were analyzed by analysis
1275 of variance with the post hoc Tukey or Bonferroni multiple comparison test. Data of three
1276 groups over time were analyzed by two way analysis of variance with the post hoc Tukey
1277 multiple comparison test. Analysis of two samples was performed with two-tailed Student's t-
1278 test, Mann-Whitney t test and statistics for HCC incidence were calculated using two-tailed
1279 Fisher's exact test. Statistical significance is indicated either as exact p-value or as follows:*p
1280 < 0.05, **p < 0.01, ***p < 0.001, , and ****p < 0.0001; “n.s.” indicates not significant.

1281

1282 **Data availability Statement**

1283 Data that support the findings of this study have been deposited in uploaded to ArrayExpress
1284 (www.ebi.ac.uk/arrayexpress/) and the data set is available under the accession number E-
1285 MTAB-6073, entitled "Transcriptomic differences in livers of mice fed with normal diet and
1286 choline-deficient high-fat diet".

1287 Moreover, the data that support the findings of this study are available from the
1288 corresponding authors upon reasonable request. If not stated otherwise, the authors declare
1289 that all other data supporting the findings of this study are available within the paper and its
1290 supplementary information files.

1291 The Figures 6a and Supplementary Fig. 12 have associated source data that are uploaded to
1292 ArrayExpress (www.ebi.ac.uk/arrayexpress/) and the data set is available under the
1293 accession number E-MTAB-6073, entitled "Transcriptomic differences in livers of mice fed
1294 with normal diet and choline-deficient high-fat diet".

1295 **References**

- 1296 61. Bender, M., Hagedorn, I. & Nieswandt, B. Genetic and antibody-induced glycoprotein
 1297 VI deficiency equally protects mice from mechanically and FeCl(3) -induced
 1298 thrombosis. *J Thromb Haemost* **9**, 1423-1426 (2011).
- 1299 62. Tiedt, R., Schomber, T., Hao-Shen, H. & Skoda, R.C. Pf4-Cre transgenic mice allow
 1300 the generation of lineage-restricted gene knockouts for studying megakaryocyte and
 1301 platelet function in vivo. *Blood* **109**, 1503-1506 (2007).
- 1302 63. World Medical Association Declaration of Helsinki. Recommendations guiding
 1303 physicians in biomedical research involving human subjects. *Cardiovasc Res* **35**, 2-3
 1304 (1997).
- 1305 64. International Conference on Harmonisation of technical requirements for registration
 1306 of pharmaceuticals for human, u. ICH harmonized tripartite guideline: Guideline for
 1307 Good Clinical Practice. *J Postgrad Med* **47**, 45-50 (2001).
- 1308 65. Directive 2001/20/EC of the European Parliament and of the Council of 4 April 2001
 1309 on the approximation of the laws, regulations and administrative provisions of the
 1310 member states relating to the implementation of good clinical practice in the conduct
 1311 of clinical trials on medicinal products for human use. *Med Etika Bioet* **9**, 12-19
 1312 (2002).
- 1313 66. Grundy, S.M., *et al.* Implications of recent clinical trials for the National Cholesterol
 1314 Education Program Adult Treatment Panel III guidelines. *Circulation* **110**, 227-239
 1315 (2004).
- 1316 67. Werner, M., *et al.* All-In-One: Advanced preparation of Human Parenchymal and Non-
 1317 Parenchymal Liver Cells. *PLoS One* **10**, e0138655 (2015).
- 1318 68. Maaten, L.J.P.v.d. & Hinton, G.E. Visualizing High-Dimensional Data Using t-SNE.
 1319 *Journal of Machine Learning Research* **9**, 2579-2605 (2008).
- 1320 69. Raasch, J., *et al.* I kappa B kinase 2 determines oligodendrocyte loss by non-cell-
 1321 autonomous activation of NF-kappaB in the central nervous system. *Brain* **134**, 1184-
 1322 1198 (2011).
- 1323 70. Bergmeier, W., *et al.* Flow cytometric detection of activated mouse integrin
 1324 alphaIIb beta3 with a novel monoclonal antibody. *Cytometry* **48**, 80-86 (2002).
- 1325 71. Schulte, V., *et al.* Targeting of the collagen-binding site on glycoprotein VI is not
 1326 essential for in vivo depletion of the receptor. *Blood* **101**, 3948-3952 (2003).
- 1327 72. Nieswandt, B., *et al.* Long-term antithrombotic protection by in vivo depletion of
 1328 platelet glycoprotein VI in mice. *J Exp Med* **193**, 459-469 (2001).
- 1329 73. Gruner, S., *et al.* Multiple integrin-ligand interactions synergize in shear-resistant
 1330 platelet adhesion at sites of arterial injury in vivo. *Blood* **102**, 4021-4027 (2003).
- 1331 74. Nieswandt, B., Bergmeier, W., Rackebrandt, K., Gessner, J.E. & Zirngibl, H.
 1332 Identification of critical antigen-specific mechanisms in the development of immune
 1333 thrombocytopenic purpura in mice. *Blood* **96**, 2520-2527 (2000).
- 1334 75. May, F., *et al.* CLEC-2 is an essential platelet-activating receptor in hemostasis and
 1335 thrombosis. *Blood* **114**, 3464-3472 (2009).
- 1336 76. Subramanian, A., *et al.* Gene set enrichment analysis: a knowledge-based approach
 1337 for interpreting genome-wide expression profiles. *Proceedings of the National*
 1338 *Academy of Sciences of the United States of America* **102**, 15545-15550 (2005).
- 1339 77. Parekh, S., Ziegenhain, C., Vieth, B., Enard, W. & Hellmann, I. The impact of
 1340 amplification on differential expression analyses by RNA-seq. *Sci Rep* **6**, 25533
 1341 (2016).
- 1342 78. Macosko, E.Z., *et al.* Highly Parallel Genome-wide Expression Profiling of Individual
 1343 Cells Using Nanoliter Droplets. *Cell* **161**, 1202-1214 (2015).
- 1344 79. Love, M.I., Huber, W. & Anders, S. Moderated estimation of fold change and
 1345 dispersion for RNA-seq data with DESeq2. *Genome Biol* **15**, 550 (2014).
- 1346 80. Kuleshov, M.V., *et al.* Enrichr: a comprehensive gene set enrichment analysis web
 1347 server 2016 update. *Nucleic Acids Res* **44**, W90-97 (2016).

- 1348 81. Levin, Y.S., *et al.* Effect of echo-sampling strategy on the accuracy of out-of-phase
1349 and in-phase multiecho gradient-echo MRI hepatic fat fraction estimation. *J Magn*
1350 *Reson Imaging* **39**, 567-575 (2014).
- 1351 82. Merkle, E.M. & Nelson, R.C. Dual gradient-echo in-phase and opposed-phase
1352 hepatic MR imaging: a useful tool for evaluating more than fatty infiltration or fatty
1353 sparing. *Radiographics* **26**, 1409-1418 (2006).
- 1354 83. Nombela-Arrieta, C., *et al.* Quantitative imaging of haematopoietic stem and
1355 progenitor cell localization and hypoxic status in the bone marrow microenvironment.
1356 *Nat Cell Biol* **15**, 533-543 (2013).
- 1357 84. Thon, J.N. & Italiano, J.E. Platelets: production, morphology and ultrastructure.
1358 *Handb Exp Pharmacol*, 3-22 (2012).
- 1359 85. Thon, J.N. & Italiano, J.E., Jr. Does size matter in platelet production? *Blood* **120**,
1360 1552-1561 (2012).

1361

1362

1363 **ACKNOWLEDGMENTS**

1364 We thank Danijela Heide, Jenny Hetzer, Ruth Hillermann, Corinna Gropp, Florian
1365 Müller, Sandra Prokosch, Daniel Kull, Reiner Dunkl, Olga Seelbach, Marion Bawohl,
1366 Renaud Maire, Monika Bieri, Christiane Mittmann, Hanna Honcharova-Biletska,
1367 André Fitsche, Arlind Adili, Patrick Münzer, Trecia Nussbaumer, Fabiola Prutek,
1368 Gopuraja Dharmalingam and Indrabahadur Singh for excellent technical assistance.
1369 We thank Konstantin Nikolaou for the help regarding the human cohort recruitment
1370 and analysis. M.M. was partially supported by grants from the University Zurich
1371 (Zurich Integrative Human Physiology (ZHIP) Sprint Fellowship) and from the
1372 Hartmann Müller Stiftung, Zurich. **A.W. was supported by a grant from the Swiss**
1373 **National Science Foundation (320030_182764).** M.Heikenwaelder. was supported by
1374 an ERC Consolidator grant (HepatoMetaboPath), **an EOS grant**, the SFBTR 209 and
1375 SFBTR179 and the Helmholtz-Gemeinschaft, Zukunftsthema "Immunology and
1376 Inflammation" (ZT-0027). This project has received funding from the European
1377 Union's Horizon 2020 research and innovation program under grant agreement No
1378 667273 and the DFG (SFB/TR 240 to B.N., D.S.). ERC Consolidator grant
1379 "CholangioConcept" (to L.Z.), the German Research Foundation (DFG): grants
1380 FOR2314, SFB685 and the Gottfried Wilhelm Leibniz Program (to L.Z.). Further
1381 funding was provided by the German Ministry for Education and Research (BMBF)
1382 (eMed/Multiscale HCC), the German Universities Excellence Initiative (third funding
1383 line: 'future concept'), the German Center for Translational Cancer Research (DKTK)
1384 and the German-Israeli Cooperation in Cancer Research (DKFZ-MOST) (to L.Z.). D.I.
1385 was supported by an EMBO Long-term Fellowship. JML is supported by Asociación
1386 Española Contra el Cáncer, Spanish National Health Institute (SAF2013-41027),
1387 Generalitat de Catalunya (SGR 1162), Samuel Waxman Cancer Research
1388 Foundation, and US Department of Defense (CA150272P3). D.A.M. is supported by

1389 CRUK grant C18342/A23390 and MRC grant MR/K001949/1. MP is supported by the
1390 German Research Foundation (DFG). J.M.L. is supported by grants from the
1391 European Commission Horizon 2020 Program (HEPCAR, proposal number 667273-
1392 2), the US Department of Defense (CA150272P3), the National Cancer Institute (P30
1393 CA196521), the Samuel Waxman Cancer Research Foundation, the Spanish
1394 National Health Institute (SAF 2016-76390), Asociación Española Contra el Cáncer
1395 (Accelerator award: HUNTER), the Generalitat de Catalunya (AGAUR, SGR-1358).
1396 M.G., T.G. and D.R. was supported by grants of the German Research Foundation
1397 (KFO274 and TR-SFB240). D.J.W. received Wellcome Trust Strategic Award
1398 (098565/Z/12/Z) and funding from the Medical Research Council (MC-A654-5QB40).
1399 C.L.W. was funded by CRUK project Cancer Research UK Programme Grant
1400 C18342/A23390.

1401

1402 **AUTHOR CONTRIBUTIONS**

1403 Design of the study: M.Malehmir, M.J.W., D.R., A.W., B.N., M.G. and M.
1404 Heikenwaelder. M.Malehmir, E.K., D.P., V.L., M.J.W., C.D., performed breeding and
1405 housing of mice. M.Malehmir, S.G., M.Szydłowska, E.K., D.P., V.L., D.I., A.A., M.P.,
1406 B.G.J.S., A.O., C.D., J.V., D.S., D.D., C.L.W., P.H., A.R., A.T., H.D., O.K., M.K.,
1407 C.J.W., R.B., N.A., M.E.H., L.S., M.Hinterleitner performed experiments. D.R., M.R.,
1408 F.B., T.G., M.N.B., O.B., M.N. and M.G. designed and performed the clinical case
1409 study. J.W., R.P., N.D., L.Z., D.J.W, H.G.A, H.D., D.K., F.T., P.F.L., T.O., D.J.W.,
1410 A.V., M.D.Milsom, A.J.R., R.R., P.K., P.A.K., B.N., A.W., J.M.L, M.Matter, D.A.M.,
1411 T.S., M.P., L.S. D.H.A., C.N.-A., J.L. provided tissue samples or mouse strains
1412 and/or scientific input. K.U. and T.E. performed bio-statistical analyses. All authors
1413 analyzed data. M.Malehmir, M.E.H., D.P., S.G., M.Szydłowska, P.K., B.N., M.G.,

1414 O.K., T.O., A.W., and M. Heikenwaelder wrote the manuscript, and all authors
1415 contributed to writing and provided feedback.

1416 **COMPETING FINANCIAL INTERESTS**

1417 Dr. Josep M. Llovet is receiving consulting fees from Bayer HealthCare
1418 Pharmaceuticals, Eli Lilly, Bristol-Myers Squibb, Merck, Eisai Inc, Celsion
1419 Corporation, Exelixis, Merck, Ipsen, Glycotest, Navigant, Leerink Swann LLC,
1420 Midatech Ltd, Fortress Biotech, Sprink Pharmaceuticals and Nucleix and research
1421 support from Bayer HealthCare Pharmaceuticals, Eisai Inc, Bristol-Myers Squibb and
1422 Ipsen.

1423 This article presents independent research supported in part by the National Institute
1424 for Health Research (NIHR) Birmingham Biomedical Research Centre. The views
1425 expressed are those of the author(s) and not necessarily those of the National Health
1426 Service, the NIHR, or the Department of Health.

1427 The authors declare no competing financial interests.

1428

1429

1430 **FIGURE LEGEND**

1431 **Figure 1: Increased platelet numbers and aggregates in liver sinusoids of murine and**
1432 **human NASH.**

1433 **(a)** CD42b staining and quantification of intrahepatic platelets (CD42b⁺) in 6 months ND or
1434 CD-HFD fed mice, arrows indicate platelets, (n=7 mice/group), scale bar: 50 μ m. **(b)** 3D
1435 confocal images of platelet (green)/liver endothelium (grey) interaction of 6 months ND or
1436 CD-HFD fed mice (n=4 mice/group), scale bar: 20 μ m. See also Movies S1 and S2. **(c)**
1437 CD42b staining and quantification in 6 months ND, WD-HTF (n=6 mice/group) or **(d)** WD-
1438 NTF fed mice, arrows indicate platelets, (ND n=12 mice; WD-HTF n=4 mice), scale bar: 50
1439 μ m. **(e)** CD42b staining and quantification of intrahepatic platelets (CD42b⁺) in 2 months ND
1440 or MCD fed mice, arrows indicate platelets, (n=5 mice/group), scale bar: 50 μ m. **(f)** CD61
1441 staining and quantification of platelets (CD61⁺) in human livers, arrows indicate platelets,
1442 (non-diseased patients n=4; NASH patients n=21). **(g)** H/E, CD42b staining and
1443 quantification in 6 months ND or HFD-45% fed mice, (ND n=6 mice; HFD-45% n=7 mice),
1444 scale bar: 50 μ m **(h)** H/E, CD42b staining and quantification in 6 months ND or HFD
1445 (60%kcal & low sucrose (LS)) fed mice, (ND n=8 mice; HFD n=6 mice), scale bar: 50 μ m. All
1446 data are shown as mean \pm SEM. All data were analyzed by two-tailed Student's t test.

1447

1448 **Figure 2: Asp-Clo treatment results in reduction of steatosis, liver damage, NASH and**
1449 **NASH-associated conditions.**

1450 **(a)** Body weight development of 12 months ND, CD-HFD or CD-HFD/Asp-Clo fed mice (ND
1451 n=5 mice; CD-HFD n=5 mice; CD-HFD/Asp-Clo n=9). Statistic: ND vs. CD-HFD (black
1452 asterisks), ND vs. CD-HFD/Asp-Clo (green asterisks). **(b)** ALT of 12 months ND, CD-HFD or
1453 CD-HFD/Asp-Clo fed mice (6 months: ND n=14 mice; CD-HFD n=11 mice; CD-HFD/Asp-Clo
1454 n=4 mice; 12 months: ND n=7 mice; CD-HFD n=12 mice; CD-HFD/Asp-Clo n=18 mice). **(c)**
1455 IPGTT of 6 months ND, CD-HFD or CD-HFD/Asp-Clo fed mice (n=5 mice/group). Statistic:
1456 ND vs. CD-HFD (black asterisks), ND vs. CD-HFD/Asp-Clo (green asterisks). **(d)** Liver
1457 triglyceride (6 months: ND n=11 mice; CD-HFD n=15 mice; CD-HFD/Asp-Clo n=7 mice; 12
1458 months: ND n=4 mice; CD-HFD n=9 mice; CD-HFD/Asp-Clo n=15 mice) and **(e)** serum
1459 cholesterol levels of 6 and 12 months ND, CD-HFD or CD-HFD/Asp-Clo fed mice (6 months:
1460 ND n=4 mice; CD-HFD n=7 mice; CD-HFD/Asp-Clo n=9 mice; 12 months: ND n=6 mice; CD-
1461 HFD n=17 mice; CD-HFD/Asp-Clo n=11 mice). **(f)** Real-time qPCR analysis for genes
1462 involved in lipid metabolism/ β -oxidation of 6 months ND, CD-HFD or CD-HFD/Asp-Clo fed
1463 mice (ND n=4 mice; CD-HFD n=5 mice; CD-HFD/Asp-Clo n=7 mice). Statistic: CD-HFD vs.
1464 CD-HFD/Asp-Clo (green asterisks). **(g)** Analysis of VO₂ and respiratory exchange ratio

1465 (RER) over time in 2 months ND, CD-HFD or CD-HFD/Asp-Clo fed mice (ND n=4 mice; CD-
1466 HFD n=8 mice; CD-HFD/Asp-Clo n=8 mice). **(h)** Analysis of food (g/mouse/day) and water
1467 intake (ml/mouse/day) (ND n=4 mice; CD-HFD n=8 mice; CD-HFD/Asp-Clo n=6 mice). **(i)**
1468 MRI analyses 6 months ND, CD-HFD or CD-HFD/Asp-Clo fed mice (n=3 mice/group). T1
1469 (fast low-angle shot [FLASH]) OUT phase: dark color indicative of steatosis. T2 TurboRare:
1470 an increase in subcutaneous and abdominal fat and hepatic lipid accumulation (bright
1471 regions). **(j)** H/E staining and **(k)** NAS evaluation of 6 months ND, CD-HFD or CD-HFD/Asp-
1472 Clo fed mice (ND n=9 mice; CD-HFD n=9 mice; CD-HFD/Asp-Clo n=6 mice), scale bar:
1473 100µm in 10X, 50µm in 20X. All data are shown as mean ± SEM. Data in (a) and (c) were
1474 analyzed by two way analysis of variance with the post hoc Tukey's multiple comparison test;
1475 *: P < 0.05. **: P < 0.01. ***: P < 0.001. ****: P < 0.0001. Data in (b), (d), (e), (g), (h) and (k)
1476 were analyzed by one way analysis of variance with the post hoc Tukey's multiple
1477 comparison test. Data in (f) were analyzed by two-tailed Mann Whitney's test; *: P < 0.05. **: P < 0.01.

1479

1480 **Figure 3: Anti-platelet treatment with Asp-Clo abrogates immune cell infiltration into**
1481 **the liver and prevents NASH-induced HCC development.**

1482 **(a)** CD3, F4/80, MHCII and Ly-6G staining and quantification of 6 months ND, CD-HFD or
1483 CD-HFD/Asp-Clo fed mice (CD3: ND n=5 mice; CD-HFD n =11 mice; CD-HFD/Asp-Clo n=5
1484 mice; F4/80: ND n=6 mice; CD-HFD n=12 mice; CD-HFD/Asp-Clo n=5 mice; MHCII: ND n=9
1485 mice; CD-HFD n=12 mice; CD-HFD/Asp-Clo n=5 mice), scale bar: 50µm. **(b) (left)**
1486 Representative FACS plots and quantification of hepatic CD4/CD8 ratio, **(right)** NKT cells
1487 and **(c)** activated CD8⁺ cells of 6 months ND, CD-HFD or CD-HFD/Asp-Clo fed mice (CD8⁺:
1488 ND n=6 mice; CD-HFD n=6 mice; CD-HFD/Asp-Clo n=4 mice; CD3⁺NK1.1⁺: ND n=4 mice;
1489 CD-HFD n=4 mice; CD-HFD/Asp-Clo n=3 mice; CD8⁺CD62L⁺CD44⁺CD69⁺: ND n=6 mice;
1490 CD-HFD n=6 mice; CD-HFD/Asp-Clo n=4 mice). **(d)** Western blot images of 6 months ND,
1491 CD-HFD or CD-HFD/Asp-Clo fed mice (n=2 mice/group). kDa: kilo Dalton. **(e)** Representative
1492 macroscopical images of livers from 12 months ND, CD-HFD or CD-HFD/Asp-Clo fed mice.
1493 (ND n=0 tumors in 27 mice; CD-HFD n=13 tumors in 52 mice; CD-HFD/Asp-Clo n=0 tumors
1494 in 20 mice). White arrow head indicate HCC, scale bar: 7.5 mm. **(f)** HCC incidence of 12
1495 months ND, CD-HFD or CD-HFD/Asp-Clo fed mice. (T=tumor; NT=non-tumor), (ND n=0
1496 tumors in 27 mice; CD-HFD n=13 tumors in 52 mice; CD-HFD/Asp-Clo n=0 tumors in 20
1497 mice). **(g)** HCC characterization by H/E and collagen IV (Col IV) of 12 months ND, CD-HFD
1498 or CD-HFD/Asp-Clo fed mice, dashed line indicates tumor (T) border, scale bar: 2 mm (upper
1499 row H/E) and 200 µm (lower H/E; Col IV). All data are shown as mean ± SEM. Data in (a), (b)

1500 and (c) were analyzed by one way analysis of variance with the post hoc Tukey's multiple
1501 comparison test. Data in (f) were analyzed by two-sided Fisher's exact test.

1502

1503 **Figure 4: Platelets efficiently populate the liver early during fatty liver pathogenesis.**

1504 **(a)** Intravital microscopy of livers of 4, 5, 6 and 8 weeks ND or CD-HFD fed mice. Analysis of
1505 Kupffer cells (violet), platelets (blue) and granulocytes (red), (4 weeks: ND n=2 mice; CD-
1506 HFD n=2 mice; 5 weeks: ND n=2 mice; CD-HFD n=2 mice; 6 weeks: ND n=4 mice; CD-HFD
1507 n=4 mice; 8 weeks: ND n=3 mice; CD-HFD n=3 mice), scale bar: 40 μ m. **(b)** CD3 staining
1508 and quantification of 6 (ND n=4 mice; CD-HFD n=8 mice) or **(c)** 8 weeks ND or CD-HFD fed
1509 mice (ND n=5 mice; CD-HFD n=4 mice), scale bar: 50 μ m. **(d)** Quantification of platelet area
1510 by intravital microscopy of mice shown in (a) (ND: 4 weeks n=2 mice and 40 FOV; 5 weeks
1511 n=2 mice and 40 FOV; 6 weeks n=4 mice and 40 FOV; 8 weeks n=2 mice and 40 FOV; CD-
1512 HFD: 4 weeks n=2 mice and 20 FOV; 5 weeks n=2 mice and 20 FOV; 6 weeks n=4 mice and
1513 30 FOV; 8 weeks n=2 mice and 19 FOV). **(e)** Analysis of liver sinusoid diameter by intravital
1514 microscopy of mice shown in (a) (ND: 4 weeks n=2 mice and 101 sinusoids; 5 weeks n=2
1515 mice and 150 sinusoids; 6 weeks n=4 mice and 100 sinusoids; 8 weeks n=2 mice and 150
1516 sinusoids; CD-HFD: 4 weeks n=2 mice and 100 sinusoids; 5 weeks n=2 mice and 150
1517 sinusoids; 6 weeks n=4 mice and 100 sinusoids; 8 weeks n=2 mice and 100 sinusoids). **(f)**
1518 Hepatocyte swelling measurement by H/E of mice shown in (b) and (c) (6 weeks: ND n=4
1519 mice; CD-HFD n=3 mice; 8 weeks: ND n=3 mice; CD-HFD n=4 mice). **(g)** NAS evaluation of
1520 6 or 8 weeks ND or CD-HFD fed mice (6 weeks: ND n=19 mice; CD-HFD n=18 mice; 8
1521 weeks: ND n=3 mice; CD-HFD n=6 mice). **(h)** Liver triglycerides of 6 weeks ND or CD-HFD
1522 fed mice (n=3 mice/group). **(i)** 3D confocal images and quantification of platelet
1523 (green)/Kupffer cells (red) interaction of 6 months ND or CD-HFD fed mice (n=4 mice/group).
1524 Liver endothelium (grey), scale bar: 20 μ m. **(j) (left)** Representative images of intravital
1525 microscopy of 6 weeks ND or CD-HFD fed mice. Analysis of Kupffer cells (violet, violet
1526 arrowhead), HABP (red, red arrowhead) and LSECs (blue), scale bar: 43 μ m. **(right)**
1527 Representative high magnification images of intravital microscopy of mice shown in (i),
1528 Analysis of Kupffer cells (violet, violet arrowhead), HABP (red, red arrowhead) and LSECs
1529 (blue), (ND n=4 mice; CD-HFD n=4 mice), scale bar: 43 μ m. All data are shown as mean \pm
1530 SEM. All data were analyzed by two-tailed Student's t test.

1531

1532

1533

1534 **Figure 5: Intrahepatic platelet accumulation depends on Kupffer cells, hyaluronan and**
1535 **cargo function.**

1536 **(a)** Representative images of intravital microscopy after treatment (clodronate liposomes
1537 (CLL) or hyaluronidase (HYAL)) in 6 weeks ND, CD-HFD, CD-HFD +CLL or CD-HFD +HYAL
1538 fed mice. Analysis of Kupffer cells (violet), platelets (blue, blue arrowhead), and granulocytes
1539 (red), (n=4 mice/group), scale bar: 40 μ m. **(b)** H/E and F4/80 staining with quantification and
1540 NAS evaluation after treatment in 6 weeks ND, CD-HFD, CD-HFD +CLL or CD-HFD +HYAL
1541 fed mice (H/E: ND n=10 mice; CD-HFD n=14 mice; CD-HFD +CLL n=9 mice; CD-HFD
1542 +HYAL n=8 mice; F4/80: ND n=7 mice; CD-HFD n=10 mice; CD-HFD +CLL n=4 mice; CD-
1543 HFD +HYAL n=5 mice), scale bar: 50 μ m. **(c)** Quantification of platelet area by intravital
1544 microscopy of mice shown in (a) (ND n=4 mice and 40 FOV; CD-HFD n=4 mice and 30 FOV;
1545 CD-HFD +CLL n=4 mice and 40 FOV; CD-HFD +HYAL n=4 mice and 30 FOV). **(d)** ALT
1546 levels of mice shown in (b) (ND n=17 mice; CD-HFD n=13; CD-HFD +CLL n=7 mice; CD-
1547 HFD +HYAL n=8 mice). **(e-g)** H/E histology, ALT levels and NAS evaluation after anti-CD44
1548 antibody treatment (anti-CD44 antibody blocking- (KM81) or non-blocking (IM7) HA-binding
1549 site) in 6 weeks ND, CD-HFD, CD-HFD +IM7 (non-HA blocking) or CD-HFD +KM81 (HA-
1550 blocking) fed mice (ALT: ND n=16 mice; CD-HFD n=12 mice; CD-HFD +IM7 n=4 mice; CD-
1551 HFD +KM81 n=4 mice; H/E and NAS: ND n=19 mice; CD-HFD n=15 mice; CD-HFD +IM7
1552 n=4 mice; CD-HFD +KM81 n=4 mice), scale bar: 50 μ m. **(h)** Representative H/E, CD42b
1553 staining and **(i)** NAS evaluation and platelet quantification after CLL treatment in 6 months
1554 CD-HFD or CD-HFD +CLL fed mice (H/E and NAS: CD42b: CD-HFD n=5 mice; CD-HFD
1555 +CLL n=3 mice; CD42b: CD-HFD n=5 mice; CD-HFD +CLL n=3). **(j)** Body weight
1556 development of 6 months ND, CD-HFD or CD-HFD/Nbeal2^{-/-} fed mice (ND n=6 mice; CD-
1557 HFD n=6 mice; CD-HFD/Nbeal2^{-/-} n=4 mice). Statistic: ND vs. CD-HFD (black asterisks), CD-
1558 HFD vs. CD-HFD/Nbeal2^{-/-} (blue asterisks). **(k)** ALT, AST levels, **(l)** liver triglycerides and **(m)**
1559 serum cholesterol levels of mice shown in (i) (ALT: ND n=7 mice; CD-HFD n=18 mice; CD-
1560 HFD/Nbeal2^{-/-} n=4 mice; AST: ND n=4 mice; CD-HFD n=8 mice; CD-HFD/Nbeal2^{-/-} n=3 mice;
1561 liver triglycerides: ND n=5 mice; CD-HFD n=7 mice; CD-HFD/Nbeal2^{-/-} n=4 mice; serum
1562 cholesterol: ND n=4 mice; CD-HFD n=11 mice; CD-HFD/Nbeal2^{-/-} n=3 mice;). **(n)**
1563 Representative H/E of mice shown in (i) (CD-HFD n=9 mice; CD-HFD/Nbeal2^{-/-} n=10 mice),
1564 damaged hepatocytes (asterisks) are indicated, scale bar: 50 μ m. **(o)** Fat quantification by
1565 Sudan red staining of mice shown in (i) (ND n=4 mice and 17 fields; CD-HFD n=4 mice and
1566 14 fields; CD-HFD/Nbeal2^{-/-} n=4 mice and 35 fields;), scale bar: 100 μ m. All data are shown
1567 as mean \pm SEM. Data in (b), (c), (d), (f), (g), (k), (l), (m) and (o) were analyzed by one way
1568 analysis of variance with the post hoc Tukey's multiple comparison test. Data in (i) were
1569 analyzed by two-tailed Student's t test. Data in (j) were analyzed by two way analysis of

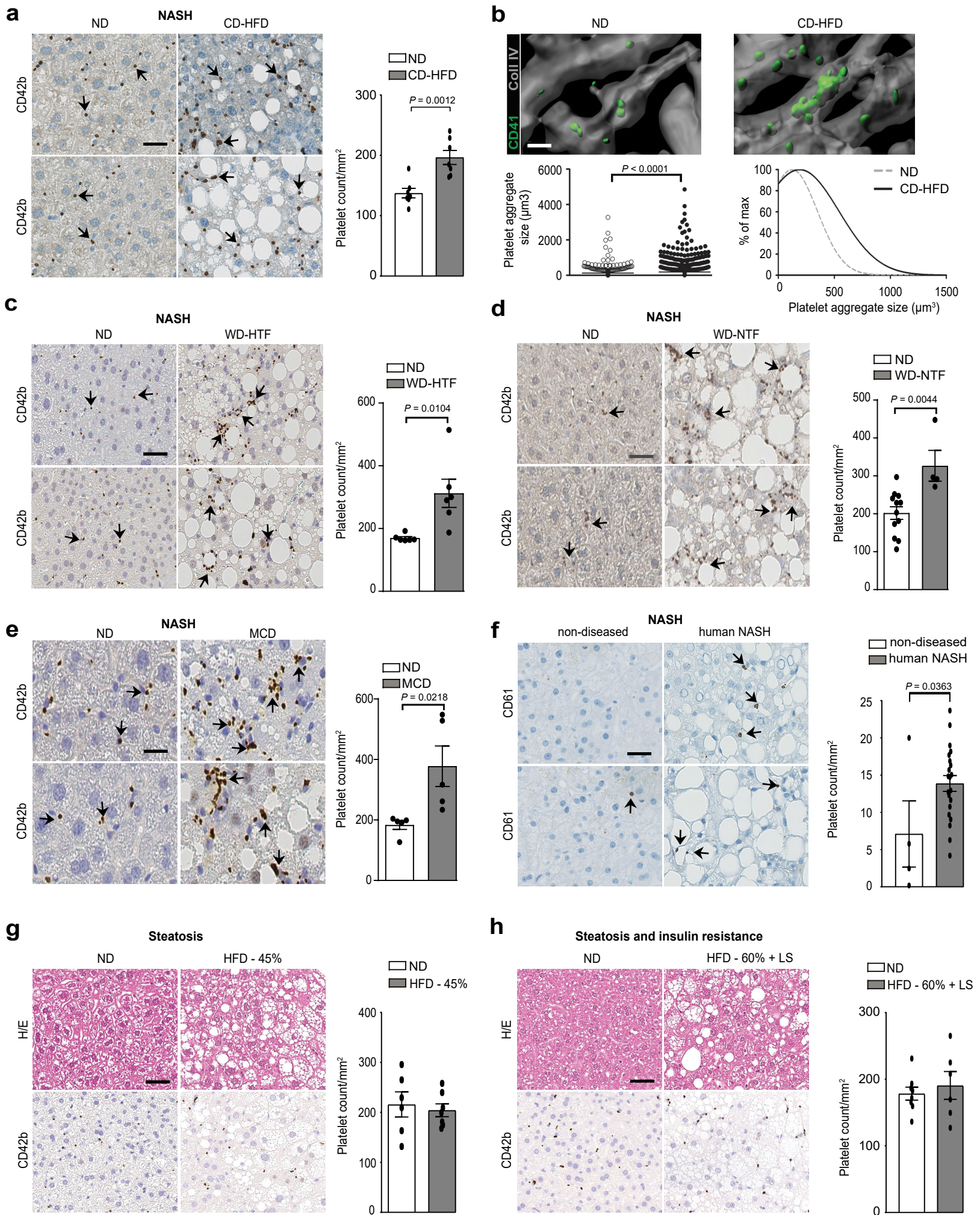
1570 variance with the post hoc Tukey's multiple comparison test; *: $P < 0.05$. **: $P < 0.01$. ***: $P <$
1571 0.001 . ****: $P < 0.0001$.

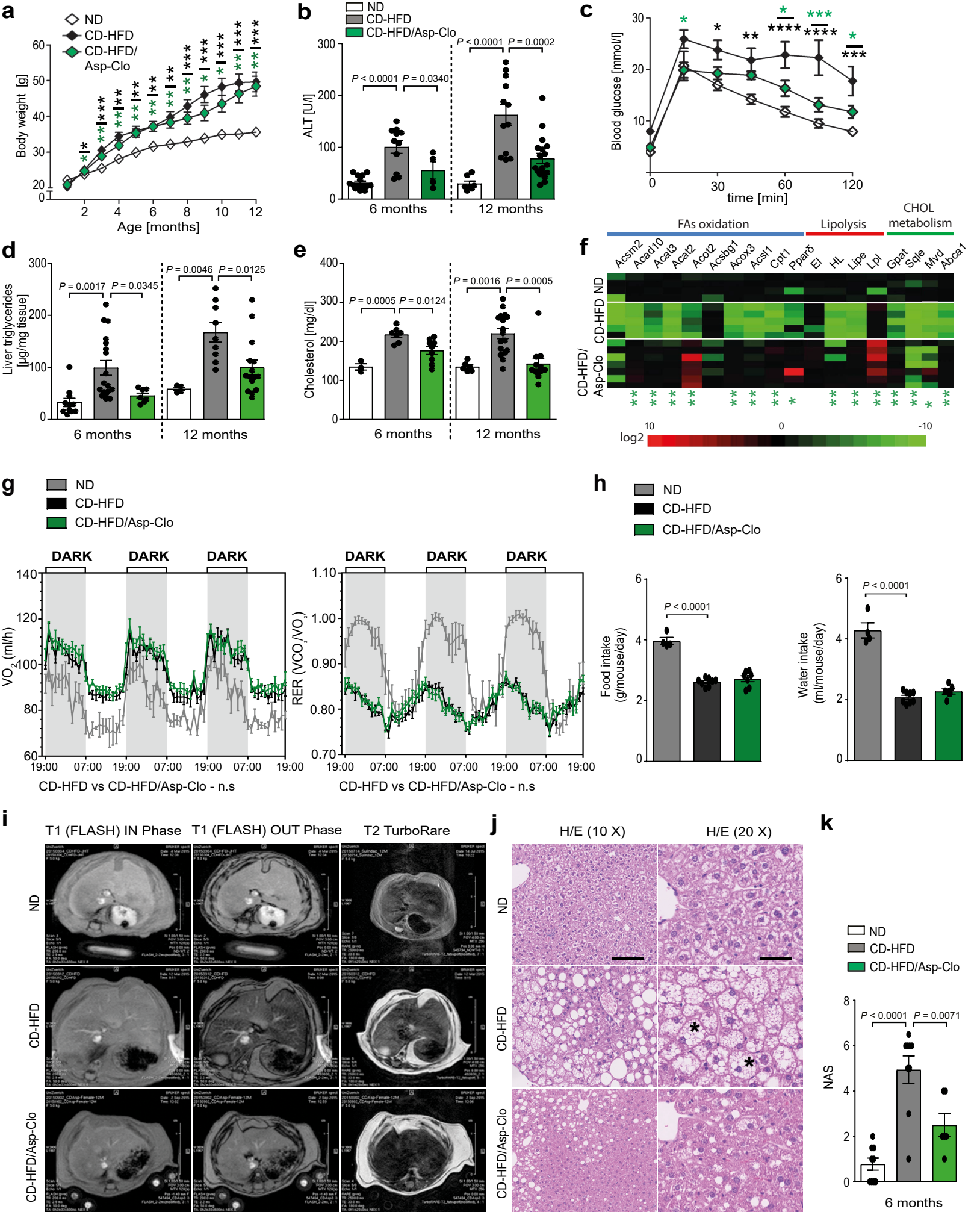
1572

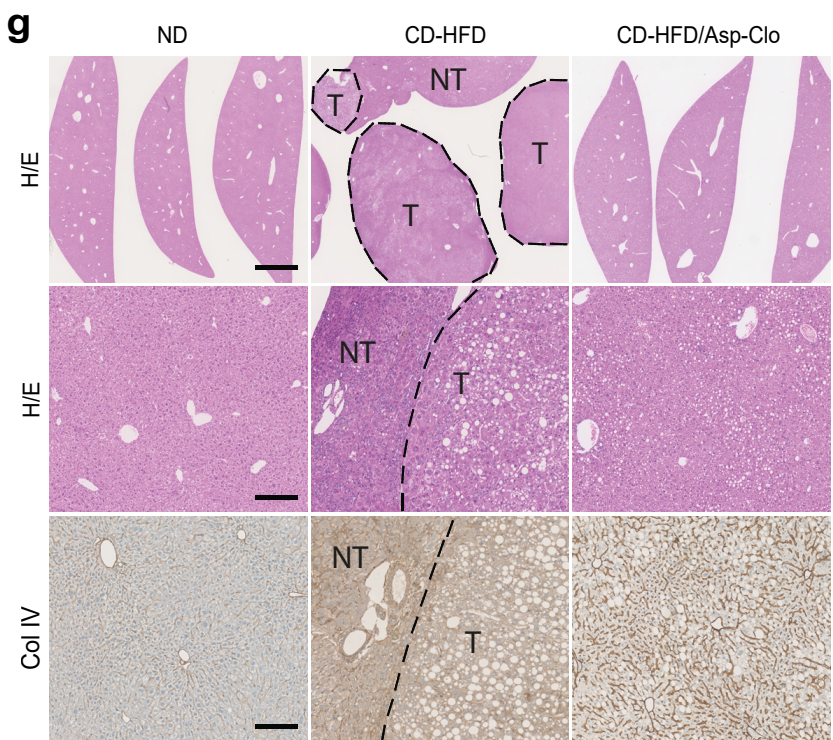
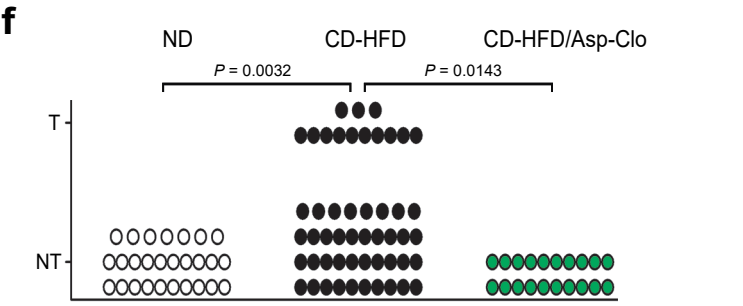
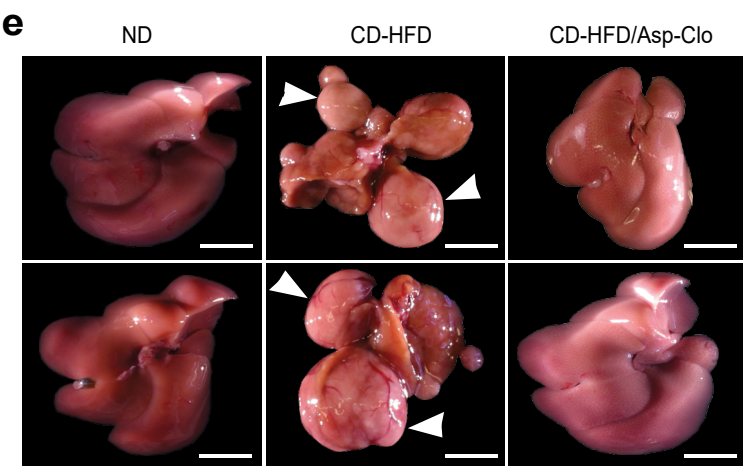
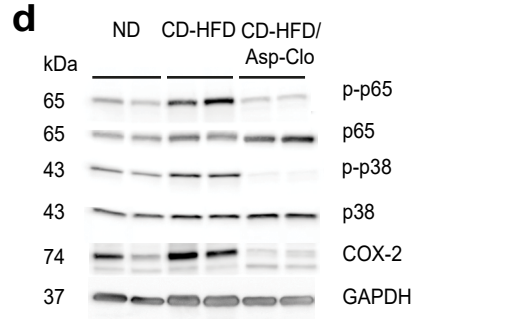
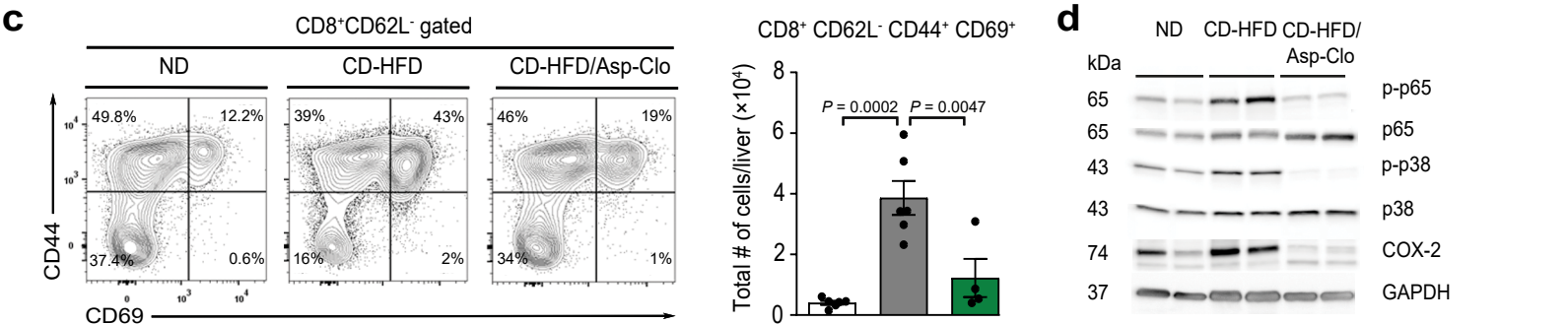
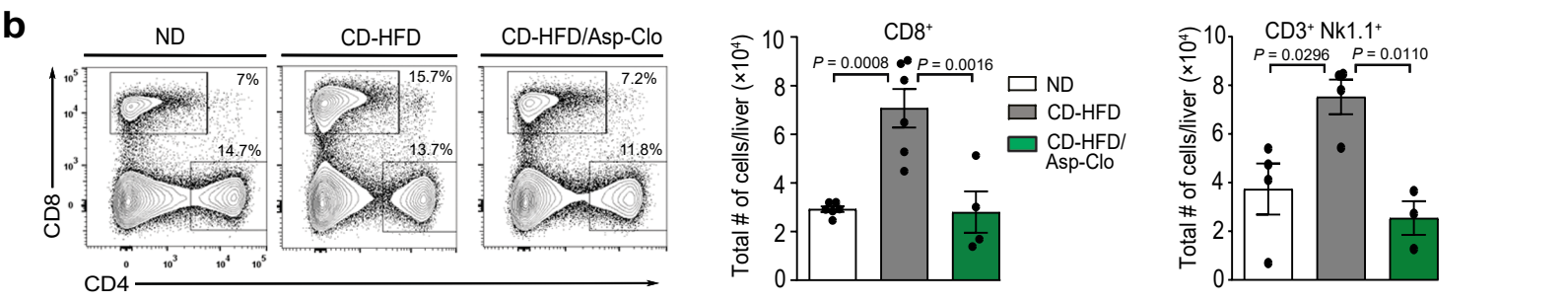
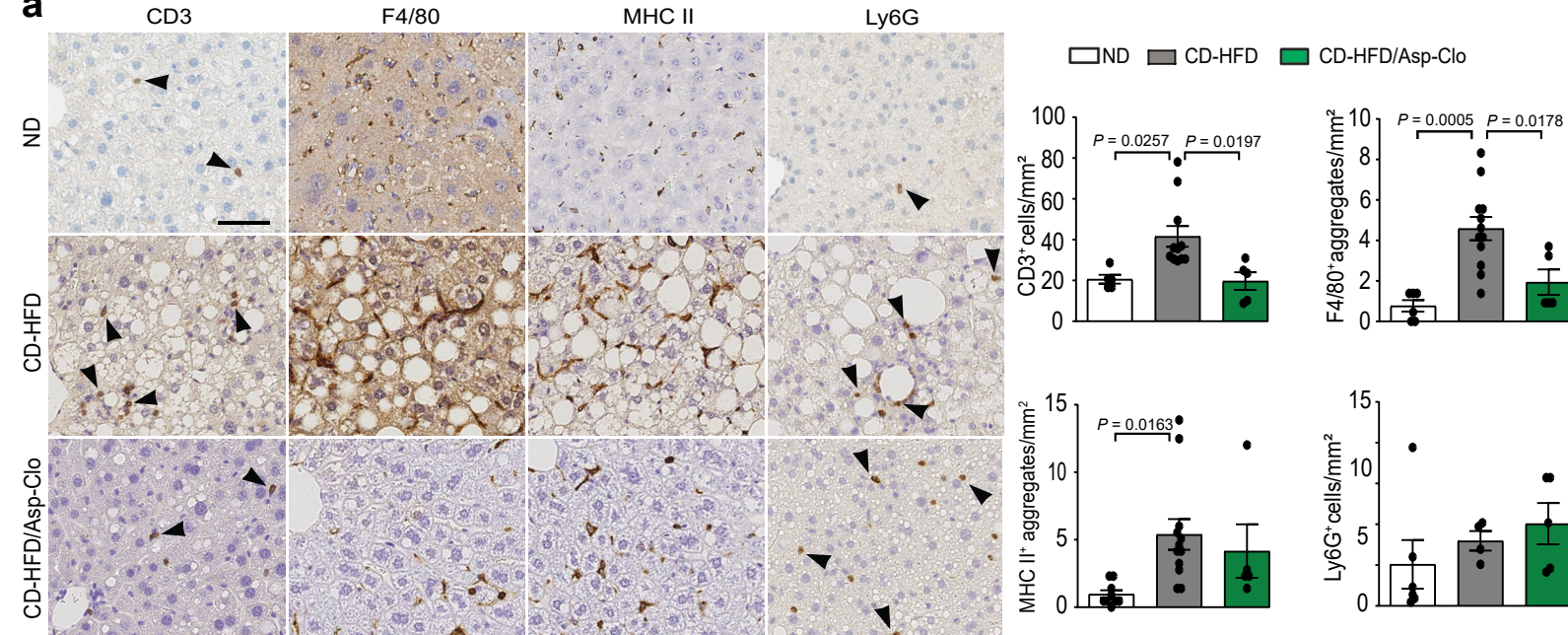
1573 **Figure 6: Anti-GPIb α antibody treatment as well as genetic dysfunction of GPIb α**
1574 **reduces NASH, fibrosis and HCC development.**

1575 **(a)** Representative 3D confocal images of GPIb α (green, green arrowheads)/Kupffer cells
1576 (red, red arrowheads) interaction of 6 months ND or CD-HFD fed mice (ND n=4 mice; CD-
1577 HFD n=4 mice). Liver endothelium (grey), scale bar: 30 μ m. **(b)** High magnification 3D
1578 confocal images and quantification of GPIb α (green)/Kupffer cells (red) and GPIb α
1579 (green)/LSECs (grey) interaction in 6 months ND or CD-HFD fed mice (ND n=4 mice and 2
1580 FOV/mouse; CD-HFD n=4 mice and 2 FOV/mouse), scale bar: 3 μ m. For visualization of
1581 intravascular events, the transparency of the sinusoidal rendering was set to 50%. **(c)**
1582 Representative H/E and CD42b staining after 5 weeks of GPIb α blocking or control Fab in 6
1583 months CD-HFD fed mice, scale bar: 50 μ m. Platelets are indicated by arrows. **(d)** Platelet
1584 quantification, **(e)** NAS evaluation, **(f)** ALT levels, **(g)** liver triglycerides and **(h)** Sirius red-
1585 positive areas quantification of mice shown in (c) (CD42b staining and platelet quantification:
1586 CD-HFD +control Fab n=8 mice; CD-HFD +GPIb α blocking Fab n=8 mice; H/E, NAS and
1587 ALT: CD-HFD +control Fab n=5 mice; CD-HFD +GPIb α blocking Fab n=4 mice; liver
1588 triglycerides: CD-HFD +control Fab n=4 mice; CD-HFD +GPIb α blocking Fab n=4 mice;
1589 Fibrosis: CD-HFD +control Fab n=5 mice; CD-HFD +GPIb α blocking Fab n=4 mice). **(i)**
1590 Serum cholesterol, liver triglycerides and **(j)** ALT levels of 6 months ND, CD-HFD or CD-
1591 HFD/*hIL4 α /GPIb α -Tg* fed mice (serum cholesterol: ND n=4 mice; CD-HFD n=5 mice; CD-
1592 HFD/*hIL4 α /GPIb α -Tg* n=4 mice; liver triglycerides: ND n=6 mice; CD-HFD n=5 mice; CD-
1593 HFD/*hIL4 α /GPIb α -Tg* n=4 mice; ALT: ND n=4 mice; CD-HFD n=3 mice; CD-
1594 HFD/*hIL4 α /GPIb α -Tg* n=4 mice). **(k)** Quantification by flow cytometry of intrahepatic immune
1595 cells (**(left)** CD8⁺ T-cells, **(middle)** activated CD8⁺ T-cells, **(right)** NKT-cells) of mice shown
1596 in (i) (CD8⁺, activated CD8⁺ and NKT cells: ND n=3 mice; CD-HFD n=3 mice; CD-
1597 HFD/*hIL4 α /GPIb α -Tg* n=4 mice). **(l)** Representative H/E staining of mice shown in (i),
1598 indications of damaged hepatocytes (asterisks) and satellitosis (arrows), scale bars: 100 μ m
1599 in 10X and 25 μ m in 40X. **(m)** Sudan red staining and **(n)** quantification of Sudan red-positive
1600 areas, **(o)** NAS evaluation of 6 months ND, CD-HFD or CD-HFD/*hIL4 α /GPIb α -Tg* fed mice
1601 (H/E and NAS: ND n=7 mice; CD-HFD n=13 mice; CD-HFD/*hIL4 α /GPIb α -Tg* n=8 mice;
1602 Sudan red staining and quantification: n=5 mice/group). **(p)** Fibrosis quantification and **(q)**
1603 Sirius red staining of 12 months ND, CD-HFD or CD-HFD/*hIL4 α /GPIb α -Tg* fed mice (H/E
1604 and NAS: ND n=7 mice; CD-HFD n=13 mice; CD-HFD/*hIL4 α /GPIb α -Tg* n=8 mice; Sudan
1605 red: n=5 mice/group; fibrosis and Sirius red: NKT cells: ND n=4 mice; CD-HFD n=9 mice;

1606 CD-HFD/*hIL4 α* /*GPIIb α* -Tg n=10 mice). **(r)** ALT levels of 12 months ND, CD-HFD or CD-
1607 HFD/*hIL4 α* /*GPIIb α* -Tg fed mice (ND n=12 mice; CD-HFD n=16 mice; CD-HFD/*hIL4 α* /*GPIIb α* -
1608 Tg n=9 mice). **(s)** Macroscopical images of tumors of mice shown in (r), tumor nodules are
1609 indicated by arrowhead) (CD-HFD: n=13 tumors in 52 mice; CD-HFD/*hIL4 α* /*GPIIb α* -Tg: n=0
1610 tumors in 24 mice), scale bar: 750 μ m. **(t)** HCC characterization by CD44v6, Collagen IV
1611 (Coll IV) and Ki67 staining form mice shown in (r). Arrowheads indicate positive hepatocytes,
1612 dashed line indicates tumor (T) border, scale bar: 200 μ m (CD44v6 and Coll IV), 50 μ m
1613 (Ki67). **(u)** HCC incidence (T=HCC; NT=non-tumor) from 12 months CD-HFD or CD-
1614 HFD/*hIL4 α* /*GPIIb α* -Tg fed mice, CD-HFD: n=13 tumors in 52 mice; CD-HFD/*hIL4 α* /*GPIIb α* -
1615 Tg: n=0 tumors in 24 mice). All data are shown as mean \pm SEM. Data in (b), (d), (e), (f), (g)
1616 and (h) were analyzed by two-tailed Student's t test. Data in (i), (j), (k), (n), (o), (p) and (r)
1617 were analyzed by one way analysis of variance with the post hoc Tukey's multiple
1618 comparison test. Data in (u) were analyzed by two-sided Fisher's exact test.







Malehmir et al., Figure 3

